**STRUCTURAL SYSTEMS**
**RESEARCH PROJECT**

Report No.

**SSRP–14/16**

# Seismic Drift Compatibility of Architectural Precast Concrete Panels and Connections: A Design Guide for Engineers

**By**

CHARLES PANKOW
FOUNDATION
Building Innovation through Research

**Tara Hutchinson, Elide Pantoli, Kurt McMullin,**

**Mark Hildebrand and Glen Underwood**

December 2014
Final Report
(Addedum 1: January 2015)

Department of Structural Engineering

University of California, San Diego
La Jolla, California 92093-0085

University of California, San Diego
Department of Structural Engineering
Structural Systems Research Project

Report No. SSRP-14/16

# Seismic Drift Compatibility of Architectural Precast Concrete Panels and Connections: A Design Guide for Engineers

by

**Tara Hutchinson** *(University of California, San Diego),*
**Elide Pantoli** *(University of California, San Diego),*
**Kurt McMullin** *(San Jose State University),*
**Mark Hildebrand** *(Willis Construction),*
**and Glen Underwood** *(Clark Pacific).*

**- Final Report -**

Department of Structural Engineering
University of California, San Diego
La Jolla, California 92093-0085
December 2014
(Addendum 1: January 2015)

# DISCLAIMER

The opinions, recommendations and conclusions contained within this report are solely those of the authors, and do not necessarily reflect the views or policies of the project sponsors. This report does not constitute a standard, specification, or regulation.

# ACKNOWLEDGEMENTS

The development of this guide was supported by the Charles Pankow Foundation Research Grant Agreement #02-11. Experimental results supporting suggestions within this guide were conducted as part of the *Building Nonstructural Components and Systems* (BNCS) project. The BNCS project is collaboration between four academic institutions (University of California, San Diego, San Diego State University, Howard University, and Worcester Polytechnic Institute), four government or granting agencies (the National Science Foundation grant CMMI-0936505, the Englekirk Advisory Board, the Charles Pankow Foundation, and the California Seismic Safety Commission), more than 40 industry partners, and two oversight committees. Many individuals contributed to the overall effort of the BNCS project. We particularly thank core team members Profs. Jose Restrepo and Joel Conte, doctoral students Rodrigo Astroza, Michelle Chen, Hamed Ebrahimian, Steven Mintz (deceased), and Xiang Wang, the NEES@UCSD and NEES@UCLA staff, Dr. Robert Englekirk, Mr. Mahmoud Faghihi, Dr. Matthew Hoehler, Prof. Ken Walsh of SDSU, and SDSU students Consuelo Aranda and Elias Espino. In addition, the input of Robert Bachman, chair of the project's Engineering Regulatory Committee, are greatly appreciated. A listing of industry project sponsors and project participants may be found on the project website: http://bncs.ucsd.edu/index.html.

To develop the present guide, the authors particularly acknowledge the support of the Precast/Prestressed Concrete Institute and its R&D Council members, who served on a technical advisory committee for the project, namely; Roger Becker (chair), Harry Gleich, Tom D'Arcy, Pat Hynes, Dave Dieter, Ed Knowles, Kim Hammon, and Doug Mooradian. The materials and technical support of Clark Pacific, Willis Construction, Regal Industries towards the testing

efforts associated with this work are greatly appreciated. Opinions and findings of this study are of the authors and do not necessarily reflect those of the sponsors.

# EXECUTIVE SUMMARY

Architectural Precast Concrete (APC) cladding has been a popular and reliable method of constructing building façades for decades. Architects, engineers, and builders have taken advantage of the high quality aesthetic finishes, the flexibility of shapes and the enhanced construction schedule that these pre-manufactured systems offer. Since the APC cladding supports exterior enclosure of the building, it is one of the essential nonstructural component and systems (NCSs) within buildings. Furthermore, these and other façades define the architectural appeal of a building and in general represent a significant portion of the cost of construction.

The APC panels are cast off-site at a precast plant, shipped to the construction site, erected with a crane, and finally fastened to the structural frame with welded and/or bolted steel connections. This panelized and jointed wall system is nonstructural in nature as it generally only supports itself and minor superimposed loads such as windows and canopies. However, the seismic mass of the system can be significant, and the limited number of connections may provide little redundancy in the event of connection failures. Furthermore, during a seismic event, the panel system will be subject to the interstory drifts imposed by the movement of the primary lateral framing system of the building. While current building codes do have design provisions addressing drift compatibility of cladding panels, these requirements are worded rather generally and leave specific detailing decisions to the judgment of the designer.

To complement current code provisions, this design guide provides a summary of the current state of practice for seismic design of APC panels and connections – with a focus on drift compatibility provisions. Its intent is to assist the precast specialty structural engineer and structural engineer of record in designing buildings with architectural precast concrete façades in areas of moderate to high seismicity. However, it may also be useful for academics and students,

architects and precast panel fabricators. In particular, quantitative recommendations, which are backed by laboratory research, are provided for achieving deformation capability of threaded rod tieback connections. Tieback connections commonly used in US practice include both sliding and flexing-type connections. Finally, the guide provides recommended design and detailing practices for *ductile* tieback connections, including a performance based ductile fuse connection that was tested within a full scale, building tested on a shake table at the University of California, San Diego. The purpose of this detail is to allow reduced panel-to-panel seismic joints at corners.

This guide is organized as follows. Chapter 1 includes an introduction to architectural precast concrete panels, their function, most common types, and practical design issues of relevance in seismic zones; Chapter 2 includes a discussion of the nature of their behavior, particularly with regard to observations from past earthquakes and key findings from recent experimental studies. Chapter 3 concludes by presenting design concepts with the intent of providing specific guidance to the engineer of such systems. This chapter concludes by presenting a numerical example demonstrating the process of designing for a ductile corner APC system.

# TABLE OF CONTENTS

# LIST OF FIGURES

# LIST OF TABLES

# ACRONYMS AND NOTATION

| | |
|---|---|
| $A_b$ | Unthreaded cross sectional area |
| ACI | America Concrete Institute |
| $A_g$ | Gross area |
| $A_{NC}$ | Projected concrete failure area of a single anchor group |
| $A_{NCO}$ | Projected concrete failure area of a single anchor |
| $a_p$ | Amplification factor |
| ASCE | American Society of Civil Engineers |
| $A_{se,N}$ | Effective cross-sectional area of anchor in tension |
| $A_t$ | Threaded cross-sectional area |
| APC | Architectural Precast Cladding |
| $A_w$ | Weld area |
| b | Width |
| BI | Base Isolated |
| BNCS | Building Nonstructural Components and Systems |
| Ca | Caulking |
| $c_{a,min}$ | Minimum distance from center of an anchor shaft to the edge of concrete |
| $c_{a1}$ | Distance from the center of an anchor shaft to the edge of concrete in one direction |
| $C_d$ | Deflection amplification factor |
| Cr | Cracking |
| d | Diameter |
| $D_p$ | Relative seismic displacement |

| | |
|---|---|
| $D_{pI}$ | Story drift |
| FB | Fixed Base |
| $f_c$’ | Uniaxial compressive strength of concrete |
| $F_{cr}$ | Critical stress |
| $F_e$ | Elastic critical buckling stress |
| $F_{EEX}$ | Electrode classification number |
| $F_n$ | Nominal stress |
| $F_p$ | Design force |
| $F_u$ | Specified minimum tensile strength |
| $f_{uta}$ | Specified tensile strength of anchor steel |
| $F_w$ | Nominal strength of the weld metal per unit area |
| $F_y$ | Specified minimum yield stress |
| $f_y$ | Specified yield strength of reinforcement |
| h | Height |
| $h_{ef}$ | Effective embedment depth of anchors |
| IP | In-Plane |
| K | Effective length factor |
| $k_c$ | Anchor parameter |
| IBC | International Building Code |
| $I_p$ | Importance factor |
| $\ell$ | Parameter for lightweight concrete |
| L | Length |

| | |
|---|---|
| $L_c$ | Rod clear length |
| $L_f$ | Rod Free Length |
| Mod. | Moderate |
| $M_n$ | Nominal flexural strength |
| $M_p$ | Plastic bending moment |
| N/A | Not available |
| $N_b$ | Basic concrete breakout strength of a single anchor in tension in cracked concrete |
| $N_{cbg}$ | Basic concre breakout strength of a group of anchors |
| NCSs | Nonstructural Components and Systems |
| NEES | Network for Earthquake Engineering Simulation |
| $N_n$ | Nominal strength in tension |
| $N_{sa}$ | Nominal strength of a single anchor or group of anchors in tension as governed by the steel strength |
| $N_{ua}$ | Factored tensile force applied to anchor or group of anchors |
| OP | Out-of-plane |
| PCI | Precast Concrete Institute |
| PFA | Peak Floor Acceleration (g) |
| PID | Peak Interstory drift (units of length) |
| PIDR | Peak interstory drift ratio (%) |
| Pm | Permanent misalignment |
| $P_{nc}$ | Compression capacity |
| $P_u$ | Require axial strength in compression |

| | |
|---|---|
| $R_n$ | Nominal strength |
| $R_p$ | Response factor |
| $R_u$ | Required strength |
| $R_y$ | Ratio of expected yield stress to the specified yield stress |
| r | Radius of gyration |
| $r_t$ | Threaded radius of gyration |
| $s_1$ | Center-to-center spacing of anchors |
| $S_{DS}$ | Design spectral response acceleration at short periods |
| t | Thickness |
| $W_p$ | Tributary weight |
| Z | Plastic section modulus |
| $\Delta_a$ | Allowable story drift |
| $\delta_x$ | Deflection at level x |
| $\delta_{xe}$ | Deflection at the level x determined by an elastic analysis |
| $\Phi$ | Resistance factor |
| $\Psi_c$ | Modification factors for cracking |
| $\Psi_{cp}$ | Modification factors for post-installed anchor |
| $\Psi_{ec}$ | Modification factors for eccentric load |
| $\Psi_{ed}$ | Modification factors for edge effects |
| 4ES | Panel installed in the $4^{th}$ floor, eastern face of the building, southern edge |
| 4SE | Panel installed in the $4^{th}$ floor, southern face of the building, eastern edge |
| 5ES | Panel installed in the $5^{th}$ floor, eastern face of the building, southern edge |
| 5SE | Panel installed in the $5^{th}$ floor, southern face of the building, eastern edge |

# 1 INTRODUCTION

## 1.1 ARCHITECTURAL PRECAST CONCRETE (APC) CLADDING

Architectural precast concrete (APC) cladding is a common façade system used to provide the architectural exterior finish to commercial, industrial, institutional, and multi-unit residential buildings. These types of façade systems are built by mounting large precast concrete panels to the structural system using steel connections. In this regard, it is noted that in the present document, *APC cladding* refers to the panel and its connectors acting as a system, whereas *APC panels* refers solely to the panels as a component. APC cladding has been a popular and reliable method of constructing building enclosures for decades. Architects, engineers, and builders have taken advantage of the high quality aesthetic finishes, the flexibility of shape, and the enhanced construction schedule that these pre-manufactured systems offer. Since the APC cladding supports exterior enclosure of the building, it is an essential type of nonstructural component and system (NCS), potentially representing a significant portion of the cost of construction. Moreover it provides architectural appeal and completeness to the building. It is noted that like many exterior façades, the APC panels are constructed off-site at a precast plant, then shipped to the construction site and erected with a crane, and finally fastened to the structural frame with welded and/or bolted connections.

## 1.2 APC CLADDING IN ZONES OF MODERATE AND HIGH SEISMICITY

The Precast/Prestressed Concrete Institute (PCI) design handbook for precast and prestressed concrete describes common types of precast concrete panels when used as cladding (PCI 2007). Generally these are categorized as solid wall panels, window panels, spandrel panels, column covers and mullions or wall-supporting units. The focus of the present design guide is on panel

systems that are capable of accommodating large story drifts by employing connections that either slide in slots or allow flexing of the connection components. Such systems are needed in zones of moderate to high seismicity. Common types of APC panels that have been successful in allowing large seismic drifts include punched window panels, u-shaped panels, or spandrel and column cover panels (schematically shown in Figure 1.1). Photographs of these systems after construction at the precast plant and as installed on a building are shown in Figure 1.2.

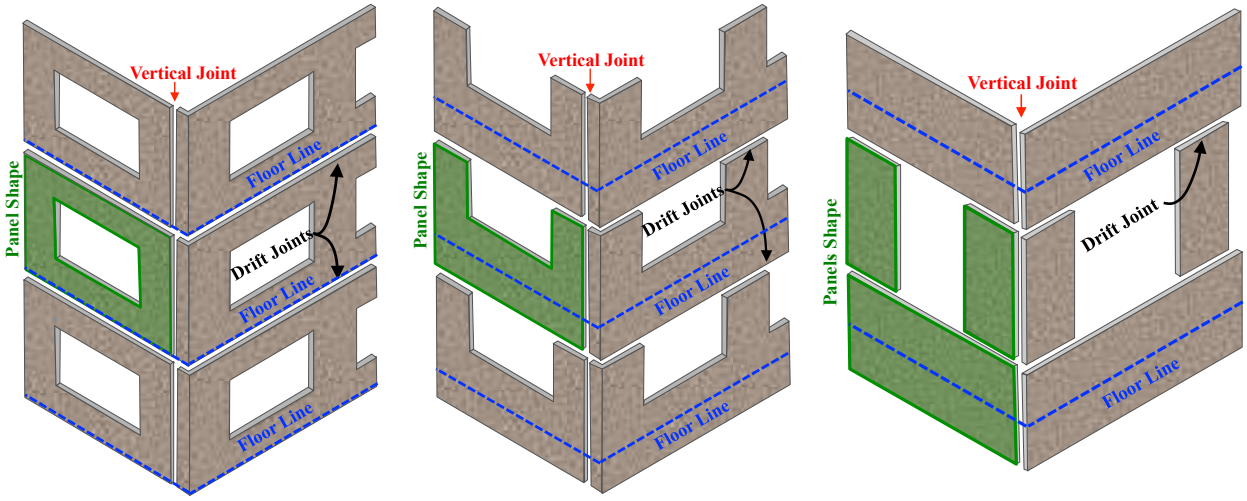


**Figure 1.1. Subset of common APC cladding arrangements for building façades: (a) punched window panels, (b) u-shaped panels, and (c) emulated u-shaped panels (also referred to as spandrel with column cover panels). These drift-compatible systems are the intended focus of this guide.**


**Figure 1.2. Examples of typical precast concrete cladding systems installed in the field: (a) punched panel system in transport and (b) u-shaped panels during installation.**

## 1.3 PUNCHED WINDOW AND U-SHAPED PANELS: PRAGMATIC ISSUES

For maximum efficiency, the precaster's goal is to panelize a façade into large repetitive shapes that take into account the visual architectural requirements and the complexity of the mold work required to fabricate the panel. Architectural constraints on panelization are floor height, horizontal module, and surface features such as joints, reveals, bullnoses, cornices and corner details. In contrast, the size of an individual panel is limited most directly by the constraints on shipping it to the job site from the factory. Punched window panels (Figure 1.1a, 1.2a) are preferred when it is possible to ship a panel whose height is equal to the distance between floors and horizontal joints at the floor are acceptable. The advantage of this configuration is that the top connections will be made above the ceiling where they are easily concealed and the panels may be pre-glazed. In contrast, u-shaped panels (Figure 1.1b) may be required if a horizontal joint at the floor is architecturally unacceptable. As a result, the top connections will be made at or below the ceiling and may be restricted in their size and location. If floor heights create panel geometries too large for transportation, then the façade system has to be broken into smaller components. By combining spandrels and column covers, a u-shape can be emulated (Figure 1.1c).

Figure 1.3 summarizes both the architectural and manufacturing aspects that guide precast designers when determining the system configuration and connection requirements. It is noted that connection types denoted towards the bottom of this flow chart are a key element to assuring the APC cladding maintains deformation compatibility with the building. As such, a detailed discussion of their design is of particular focus in the present guide and will be presented in Chapter 3.

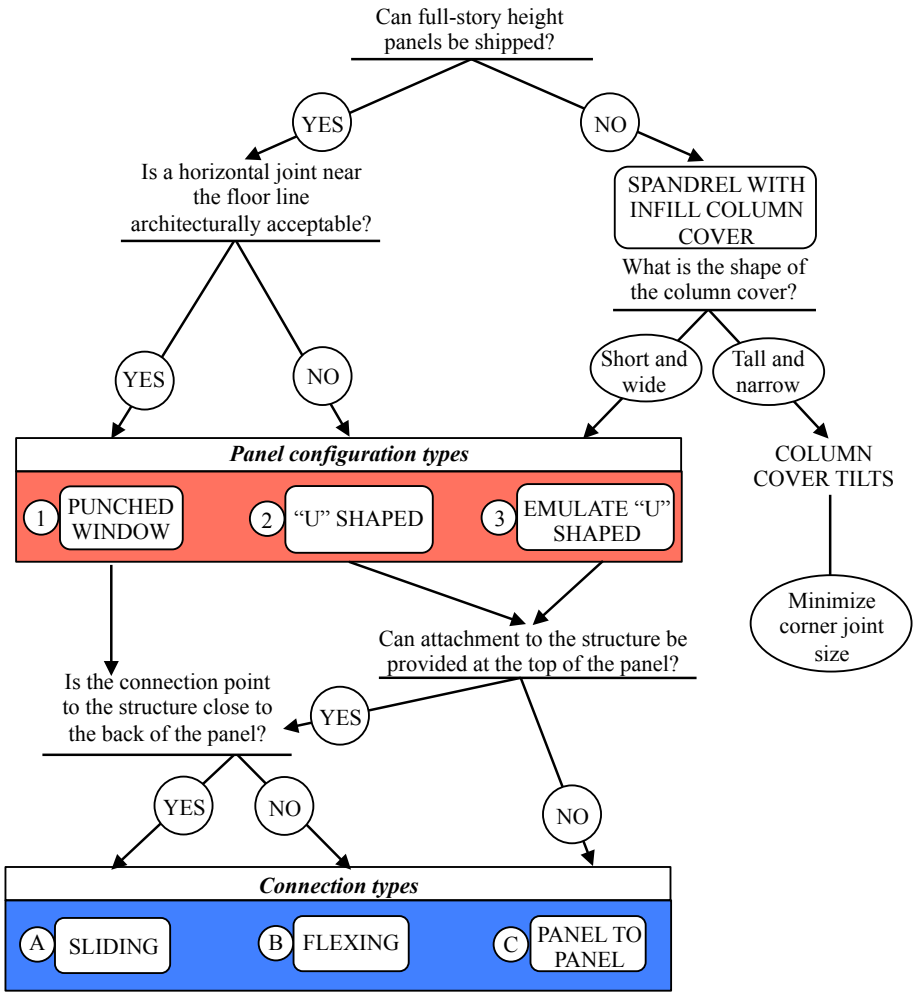


**Figure 1.3. Typical flow chart used in design of the APC cladding**

## 1.4 GOVERNING DESIGN CODES AND REFERENCE STANDARDS

The APC panels and their connections must be designed to carry anticipated loads and deformations considering demands anticipated during its intended performance period (gravity, wind, seismic and other), with sufficient margin against failure and load path continuity. At present, these systems are currently designed according to the following model code provisions and reference standards:

1. 2012 International Building Code (IBC, 2012);

2. ASCE/SEI 7-10 Minimum Design Loads for Buildings and Other Structures (ASCE, 2010);
3. ACI 318-11 – Building Code Requirements for Structural Concrete (ACI, 2011);
4. PCI MNL 120 – PCI Design Handbook (PCI, 2010);
5. PCI MNL 122 – Architectural Precast Concrete (PCI, 2007);

While load estimates are reasonably discussed within the aforementioned documents, design provisions addressing drift compatibility of cladding panels, which is essential to minimize overload and damage to the panels, are either too vague or overly qualitative to provide specific guidance to design professionals detailing these systems. Specifically, ASCE 7-10 requires that "*Connections and panel joints shall allow for the story drift caused by relative seismic displacements . . .* " and "*Connections to permit movement in the plane of the panel for story drift shall be sliding connections using slotted or oversize holes, connections that permit movement by bending of steel, or other connections that provide equivalent sliding or ductile capacity*." To satisfy these requirements it is common practice to do two things:

1. Connections intended to resist out of plane forces but allow in-plane building motion are configured with either:
   A. A slot long enough to allow maximum building motion in both directions, i.e. design a **slotted connection;**
   B. A long connection rod capable of bending enough to allow maximum building motion in both directions, i.e. design a **flexing connection;**
2. Panel joints are sized so that no panel contacts any other panel or portion of the structure while the structure experiences its maximum design seismic displacement.

Since APC panels are extremely rigid in-plane, designers must also ensure that the panels do not become part of the load path for seismic forces originating in the structure. To achieve these goals, the bottom and top of the APC panels use two different types of connections to the structural elements. The lower connections - commonly termed *bearings* - fix the bottom of the panel to the lower floor slab or beam. The top connections restrain the panel at the upper slab or beam in the out-of-plane direction, while allowing relative movement between the two in the in-plane direction. For this reason, these connections are termed *push-pull connections* or *tiebacks*. The combination of lower bearing connections and upper push-pull connections creates a panel that moves rigidly with the bottom slab in the in-plane direction, while deforming only in the out-of-plane direction. It is noted that this connection configuration can be reversed as well, with panels that hang from top bearings and have bottom push-pull connections. Regardless of the arrangement, this type of drift-absorbing mechanism, which was termed "*swaying"* by Wang (1987), creates a method for seismically protecting the panel by allowing its movement relative to the building frame. It is noted that the present terminology of *translation* or *rocking*, are more readily referred to than the original concept of *swaying*, to emphasize the rigid body movement of the panel. The concept of drift accommodation via *rocking* is more common in countries outside of the U.S. The key components of this mechanism are the push-pull connections, whose main element is a threaded rod that allows the in-plane displacement by either flexing (*flexing connection*) or sliding inside a slot (*sliding connection*) (PCI 2007).

### 1.4.1 Need for a Seismic Accomodation Joint

Implementation of a mechanism that allows drift compatibility with the building structural system results in the need for large joints at the corners of a building where the relative motion of the panels on each side of the corner would cause the panels to collide if a standard joint were

used. This collision could result in connection failure and disengagement of the panel from the structure. This seismic motion consideration has led to the use of large sealant joints running vertically up each corner of the building (Figure 1.4), a facet of the design, which is architecturally undesirable. Until the 1990's, a ¾-inch joint at this intersection was expected to perform suitably, however, code changes have resulted in seismic joint widths that match the maximum expected inelastic drift of the structure. In recent code editions for example, a flexible moment frame system may allow story drifts as large as 2-2.5% times the floor-floor height (ASCE 7-10, 2010). As a result, a joint width of 3-½" is not uncommon. While this is an aesthetically undesirable solution to architects or owners, the current state of knowledge prevents reducing the joint back to its' ¾-inch size. Revisions in this detail requirement have made the market for precast concrete cladding less desirable when compared with other façades, such as steel stud systems.

As an alternative to providing a large seismic joint, the design can allow for panels to collide. If this is to occur however, it is important to assure that the connections within the load path are not overloaded. Such a philosophy requires an element within the load path to yield and retain sufficient post-yield deformation and strength during the remainder of the seismic event. In later sections of this guide, the concept of a ductile corner connection is presented in support of such an alternative design.

**(a)** **(b)**

**Figure 1.4. Variation in reveal at the exterior of various APC cladding for (a) a miter joint and (b) a butt-return joint**

### 1.4.2 Design Community Perspective

Although design guidance for detailing these connections is not well formulated, a survey of 13 precast producers and/or designers conducted by the authors indicated that engineers certainly realize that building displacements affect panel joint size and configuration. To define the joint width and design the connections, the designer typically uses the displacement values given by the structural engineer of record or maximums allowed by the code (ASCE 7-10, 2010). More than 90% of the respondents to this survey use slotted connections to accommodate this drift, with the slots designed to take the maximum expected displacement, with nominal extra space to account for fit up tolerances. Only about 25% of respondents, however, indicated that they use flexural yielding of steel to accommodate drift even though this is expressly permitted by the code.

## 1.5 SCOPE OF THIS GUIDE

Through funding provided by the Charles Pankow Foundation and with the guidance of an industry board composed of experts in the precast concrete industry, researchers at the University of California, San Diego and San Jose State University collaborated with experts in the field of precast concrete cladding design and construction to develop the present design guide. This guide is intended for practicing structural engineers and precast specialty structural engineers designing buildings and cladding systems with architectural precast concrete panels in areas of moderate to high seismicity. Particular focus is given to APC cladding systems intended for accommodating building-induced seismic drifts and described in Figure 1.1. It is noted that design of multi-story panel systems, rocking column cover systems, and other façade types are beyond the scope of this guide. However, the fundamental principles developed herein are readily adoptable to such systems if bolted sliding connections or flexing rods connections are used. Moreover, this guide is intended for use with systems designed within moderate to high seismic zones (seismic design category C, D, E, or F according to ASCE 7-10).

# 2 NATURE OF APC CLADDING BEHAVIOR

A panelized APC cladding system is nonstructural in nature, generally supporting only its own weight and minor superimposed loads such as those from attached windows and canopies. However, the mass of the system is significant, and the discrete number of connections provides limited redundancy or alternate load paths in the event of connection failures. Furthermore, during a seismic event, the cladding system will respond to the displacement of the structure as it reacts to seismic forces. This interaction may cause adjacent panels to collide if the joints between the panels are too small (Figure 2.1). This could result in damage to the panels or their connections to the structure. Large joints, however, may compromise the building envelope or the architectural appearance of the system.

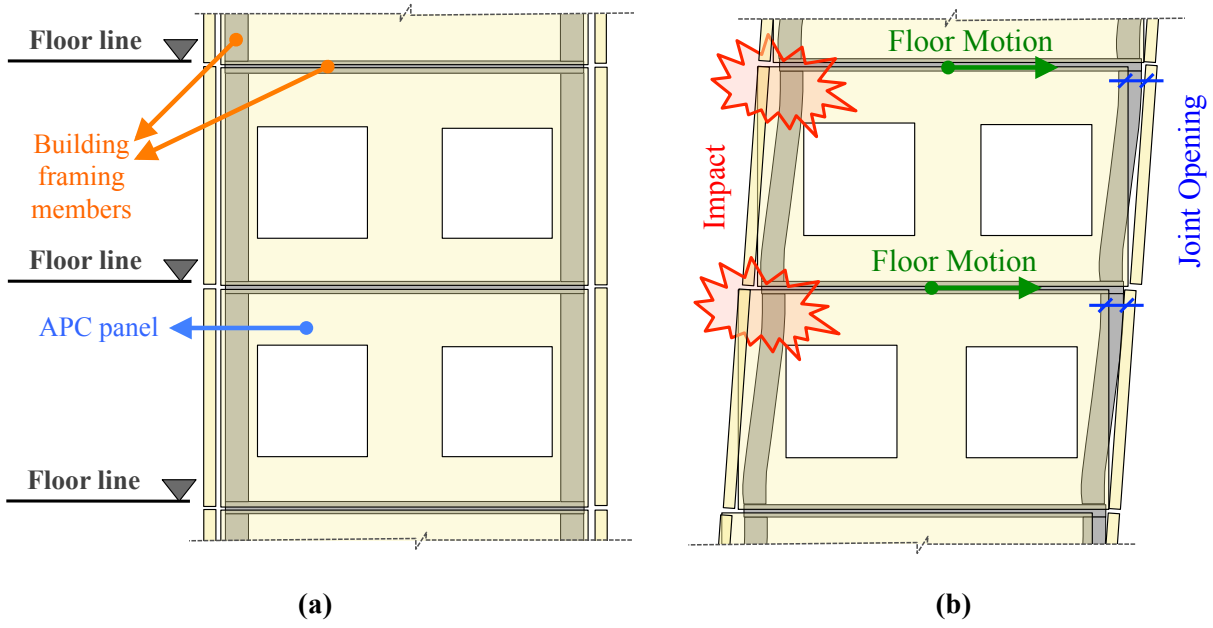


**Figure 2.1. APC cladding attached to a building frame (a) undeformed and (b) deformed during seismic displacement.**

## 2.1 OBSERVATIONS FROM PAST EARTHQUAKES

Although few significant problems have been observed in past earthquakes for APC cladding systems, it is not clear that those designed to modern codes have been subjected to a major (design or maximum credible) earthquake in the United States (U.S.). In particular, given the significant number of existing buildings with APC cladding in the U.S., panel collapse due to earthquakes has only been reported in a few cases. Precast concrete cladding panel failures were observed during the 1964 Alaska earthquake and the 1987 Whittier narrows earthquake (Figure 2.2). However, it is noted that although the 1989 Loma Prieta earthquake did not result in damage to the panels, reconnaissance teams speculate that if the intensity of the shaking had been any higher, damage to the connections would have likely occurred (EERI, 1990; and further reported in Sielaff et al., 2005). Also, no severe damage to this type of façade was reported during the 1994 Northridge earthquake (Iverson and Hawkins 1994).

**(a)** **(b)**

**Figure 2.2. APC panel (a: as installed before) and (b: fallen from a parking garage) at CSULA during the 1987 Whittier Earthquake. One person was fatally wounding (Arnold, 2009 after Taly, 1988).**

In contrast, although the detailing varies globally, instances of damage to APC systems have been reported in several earthquakes worldwide. For example, many cases of moderate and

severe damage were reported after the 1985 Mexico earthquake (Goodno et al., 1989) and the 1995 Hyogo-Ken Nanbu earthquake in Japan (Horii et al., 1995). More recently, failures of several APC panel connections were observed following the 2009 L'Aquila earthquake in Italy (Miyamoto International, 2009) and during the Chile earthquake in 2010, when several panels collapsed in the out-of-plane direction (Gosh and Cleland 2010) (Figure 2.3). During the 2011 Christchurch earthquake in New Zealand, several panels failed due to errors in the installations of the connections (Baird et al., 2011). In addition, extensive cracking, corner crushing, residual displacement of the panels and rupture of the seal at panel interfaces were reported. Insufficient displacement capacity of the connections led to several APC panel failures during the more recent 2012 Emilia earthquake in Italy (Bournas et al. 2013). It is noted that although the connection details between the panel and building may vary in other countries, for the aforementioned post-earthquake observations the intended mechanism was one of in-plane sway, yet these systems were subject to excessive in-plane drifts leading to connection overload and failure. While these failures may manifest in out of plane panel collapse (e.g. Figure 2.3), the precursor to such a result was likely the preceding in-plane connection failure.

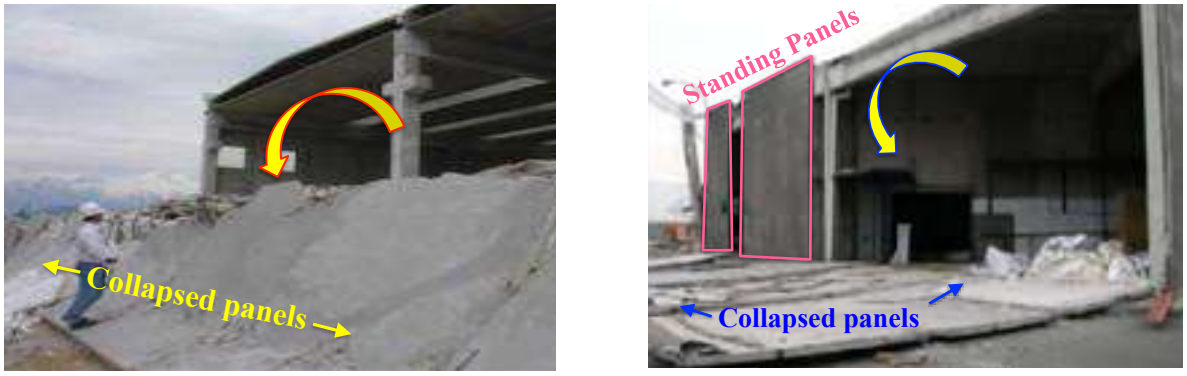


**(a)** **(b)**

**Figure 2.3. Photographs showing examples of collapsed panels after (a) the 2009 L'Aquila earthquake (Miyamoto International, 2009) and (b) the 2010 Chile earthquake (Gosh and Cleland, 2010)**

### 2.1.1 Consequence of Damage to the APC Cladding

Recent earthquakes have demonstrated that damage to any NCS in a building poses life safety hazards to occupants and may lead to significant economic losses and repair downtime. The APC cladding system is no exception as it serves as the essential exterior enclosure of a building, is heavy, and lacks redundancy. It is also important to note that façades are one of the most expensive NCSs installed on buildings (Taghavi and Miranda 2003). As a result of their limited redundancy, connection failures could destabilize the panel, threatening life-safety. Nonetheless, the building industry expectation is that these systems allow significant horizontal movement, with the cladding remaining intact and connected to the structure, even as the main structural system experiences severe damage. Indeed, improved design and detailing for the anticipated movements of the cladding is of critical importance not only because of the evidence of damage from past earthquakes, but also because of the consequences of earthquake damage to the panel system.

## 2.2 OBSERVATIONS FROM EXPERIMENTS

### 2.2.1 System-Level Investigations

Large-scale system-level experiments on buildings are costly and time consuming. However, a number of recent full-scale programs have provided an opportunity to test APC cladding in building systems. Two projects in particular are discussed in this section: the NEES/Tips project conducted at the E-Defense facility in Japan and the Building Nonstructural Components and Systems (BNCS) project at NEES@UCSD facility in the U.S..

### *NEES/Tips Project at E-Defense*

This first project was conducted in conjunction with the NEES/Tips program at the E-Defense facility in Kobe, Japan in 2011 (Ryan et al, 2008; Soroushian et al., 2012; McMullin et al., 2012). These tests were conducted on a shake table allowing motion in all six degrees of freedom. The main goal of the NEES/Tips program was the comparison of structural response of isolated buildings versus fixed-base structures and the influence on a variety of nonstructural systems including architectural precast cladding systems.

The parameters of the experiment and the performance of the building are discussed by Dao (2012), however they are provided in brevity here. The overall height of the steel moment resisting frame structure, including its foundation was 53’ with uniform story heights of 9’-6”. Lateral resistance for the building was provided by a two-bay by two-bay complete space frame with all beams and columns with moment connections. A total of 24 earthquake tests were conducted on the building, nineteen in a base isolated configuration (BI) followed by five in a fixed-base (FB) configuration.

Through support of the National Science Foundation, the Kobe, Japan-based E-Defense research facility, San Jose State University and industry professionals, a team of researchers and precast concrete producers designed and constructed architectural precast panels to American standards. Steel connections were fabricated in the United States and shipped to Japan for testing. Casting and installation of the panels was completed in Japan but used standard American practice and was observed by on-site American industry personnel. A two-panel corner assembly was constructed and attached to the 5-story steel moment frame building at levels 4 and 5. The panels were mounted on one corner of the five-story building and subjected to 3-axes of horizontal acceleration input at the base of the structure (Figure 2.4).

The size and shape of the panels were consistent with American design, although the story height is less than may be common in commercial construction. All panels were 5 inches thick and had a height of 9'-6" to match the story height. The flat panel had a width of 1'-10.5" while the corner return panel had a length of 4' and a return of 1'-10.5" as shown in Figure 2.5. The return panel weighed approximately 2.4 kips and the flat panel weighed approximately 1.1 kips. A two-inch joint separated the two panels. The two-inch joint is significantly larger than would usually be used for rocking panel systems in either U.S. or Japanese practice, however the timeline of testing did not allow for modification of the panels prior to testing.


**Figure 2.4. Upper stories of the E-Defense test building and APC panels**

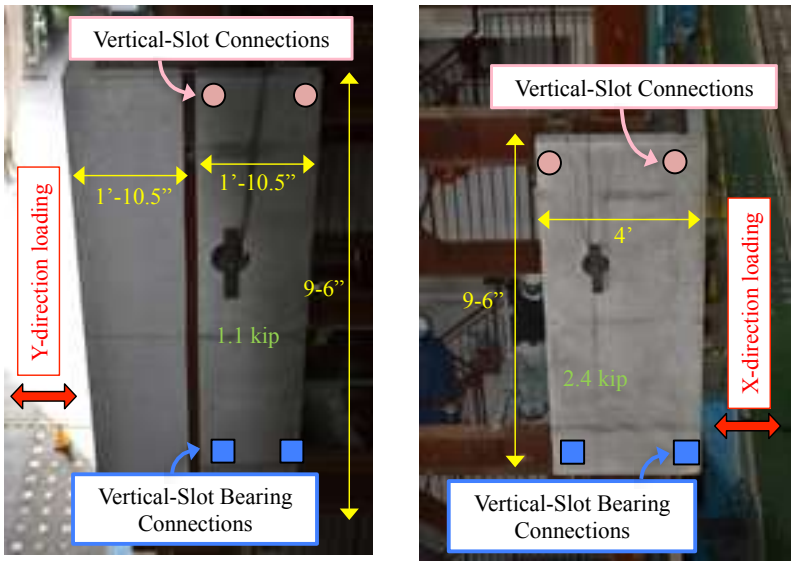


**(a)** **(b)**

**Figure 2.5. APC panel geometry and layout for the E-Defense test: (a) flat panel and (b) return panel.**

The façade design in these tests adopted a rocking action to allow lateral story drift of the building due to the use of full-story height column cover panels that had relatively narrow width. The rocking action of the panel occurs due to the use of vertical slots in all four steel connections of each panel. The vertical slots allow for relative vertical movement at the corners of the panel, which allows the top of the panel to move laterally and thus accommodate the relative lateral movement of the upper floor of the building as shown in Figure 2.6a. Two types of slotted connections were used on each panel. At the base, slotted bearing connections were used as shown in Figure 2.6b. The connection contains a vertical slot in the angles to allow upward movement but have leveling bolts that prevent the panel from moving downward, thus providing bearing support for the panel. The steel rods in the slots are unthreaded bar. The vertical angles are installed during panel installation and are welded into place after the panel is installed. Figure 2.6c shows the vertical slotted connection at the top of the panels. These top connections use threaded coil rod and were installed with zero free length (snug condition). It should be noted

that the vertical slot orientation and the panel's rocking behavior is distinctly different than the connections discussed in this design guide. However, the performance of the slotted connections in a dynamic loading environment sheds additional insight into the performance of these types of connections during seismic events.

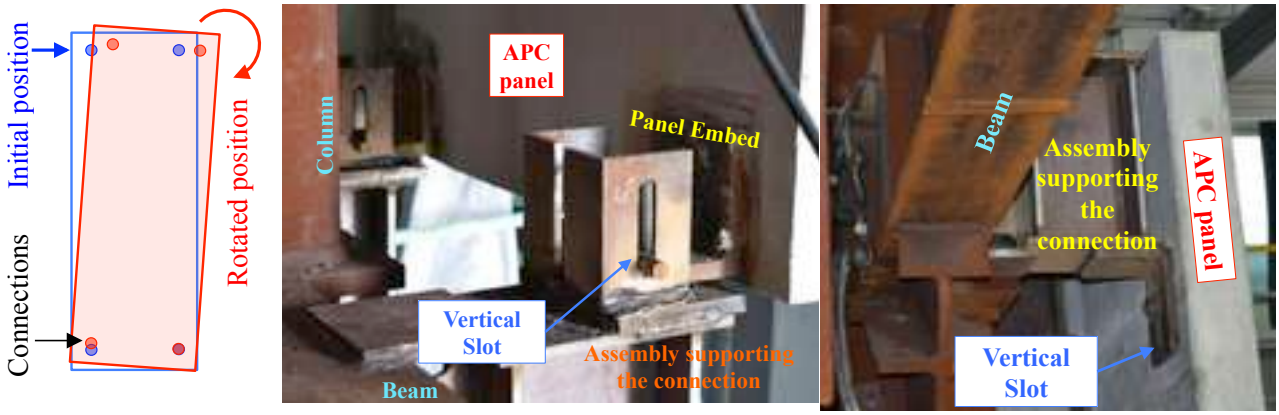


**Figure 2.6. (a) Rocking panels during their intended behavior. (b)Slotted connection used during the E-defense test at bottom – connection allows vertical movement in the upward direction of slot but leveling bolt (inside angles) prevents the connection from moving downward and (c) at top of panel. Coil rod extends through vertical slot of angle in a snug configuration. Coil nut and washer on left side of angle.**

Peak table accelerations of 0.23g in the x-direction, 0.41g in the y-direction and 1.06g in the z-direction were achieved at the base of the building during the fixed-base experiments. The peak story deflection was determined as the relative deflection of the story slabs attached to the top and bottom of the panels. Story drift ratio was determined by dividing the story deflection by the difference in the top of slab elevations of the two slabs. While the building was tested in the fixed base condition, the peak story drift ratio was 0.65% for the location of the architectural precast cladding. The largest peak story drift ratios for the base isolated structure were approximately half of this value. Visual inspection of the panels and connections occurred after each set of seismic tests where each set included approximately four different events.

Throughout the entire test program, the APC system behaved according to design, with vertical slotted connections sufficiently allowing movement to accommodate story drift and with no damage observed in any of the panels. Snug sliding connections performed without binding, allowing the panels to rack and accommodate the story drift. At the conclusion of all testing there was no visual damage to any welds, rods, panels or support plates and no permanent misalignment of the panels.

***BNCS Project at NEES@UCSD***

In 2012, a five-story full-scale building fully equipped with a large variety of NCSs was tested on the large high performance outdoor shake table at the University of California, San Diego (NEES@UCSD). It is noted that this shake table is unidirectional and imposes motion in the east-west direction. The main goal of this landmark project was to test a large number of NCSs as installed in a real building environment – by design, the specimen was intended to mimic a *total, functional* building system. The project was coined the *Building Nonstructural Components and Systems (BNCS)* project and its results are documented in a series of technical reports and papers (Chen et al., 2014, 2013a-b; Pantoli et al. 2014a, 2013a-b; Hutchinson et al., 2013). The overall height of the reinforced concrete building specimen, including its foundation, was 75', with 14' story heights. Lateral seismic resistance for this building was provided by a pair of identical one-bay special reinforced concrete moment resisting frames in the Northeast and Southeast bays. The nonstructural components and systems installed on the test specimen included stairs, a passenger elevator, various equipment at individual floors and two different types of façades: 1) the first three levels were enclosed by cold-formed steel balloon framing overlaid with synthetic stucco, and 2) the two upper levels were enclosed with a system of APC panels. An overview photograph of the building and a schematic plan view can be seen in Figure

2.7a and b, respectively. In total, thirteen earthquake tests were conducted on the building, seven while it was base isolated (BI) and six while it was in a fixed-base (FB) configuration.

Through support of the Charles Pankow Foundation and an industry advisory board within the Precast Concrete Institute (PCI), a team of researchers and precast concrete producers worked closely on the design, construction, installation, and instrumentation of the precast concrete panels installed at the upper two floors of the BNCS building specimen. Two punched window-type panels per side of the building were installed at each floor, resulting in a total of 16 panels mounted on the test building (Figure 2.7c and 2.8). Eight panels were attached so as to experience building motions predominantly in plane (IP panels) and eight experienced predominantly out of plane motions (OP panels). Connection of the panels to the building skeleton were facilitated by steel embeds installed in the slab, beams and columns. The panels were supported by bearing connections at the bottom and push-pull connections at the top. All panels were 5 inches thick. The height of the panels installed on the fourth floor was 13’11’’ while the panels on the fifth level were 15’5’’ tall. The IP panels had width between 18’8’’ and 16’11’’ and a weight between 10.7 kips and 13 kips, while the OP panels were smaller, with a width of 11’4’’ (not including the returning corner) and a weight between 8.1 and 9.5 kips. Normal weight concrete with a 28-day design compressive strength $f'_c$ = 5 ksi were used in the fabrication of these panels. The IP panels utilized four push-pull connections each in order to maximize the connections and then the details tested, however it is noted that in a real case less connections would have suffice for a panel this size. Details of the various panel geometries are summarized in Figure 2.8. The primary variables considered in the APC system of this test program included: (i) flexing and sliding push-pull connections with different rod free lengths ($L_f$) and free length-to-diameter ratios ($L_f$/d), as reported in Table 2.1; (ii) a new type of corner

connection allowing for smaller corner joints, this connection was characterized by a yielding fuse in the form of a bending plate; and (iii) miter and butt-return corner joints. All rods were type A36 steel. Material properties for the rods installed in the sliding connections is presented in Appendix A. The bending plate was constructed of ¾" thick A36 steel plate stock.

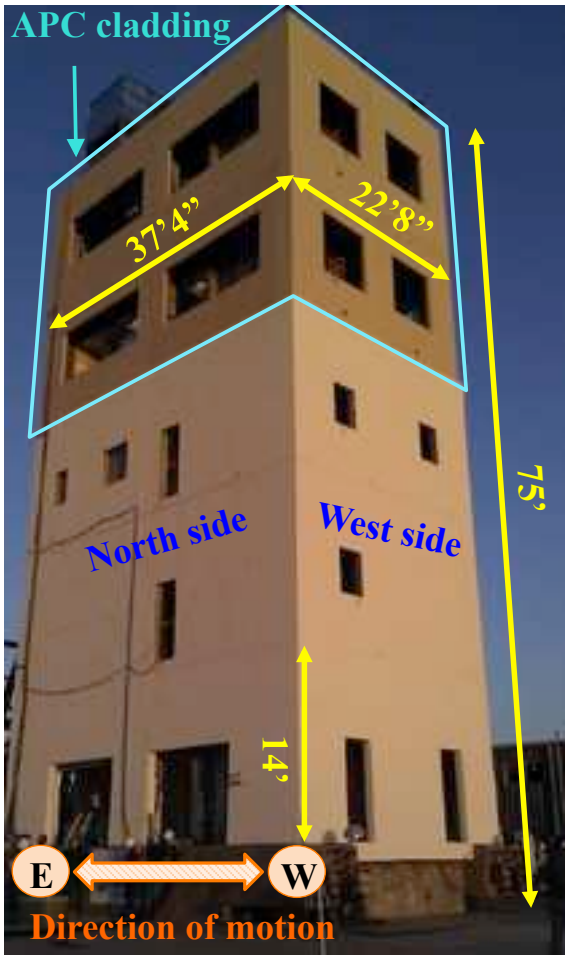


(a)

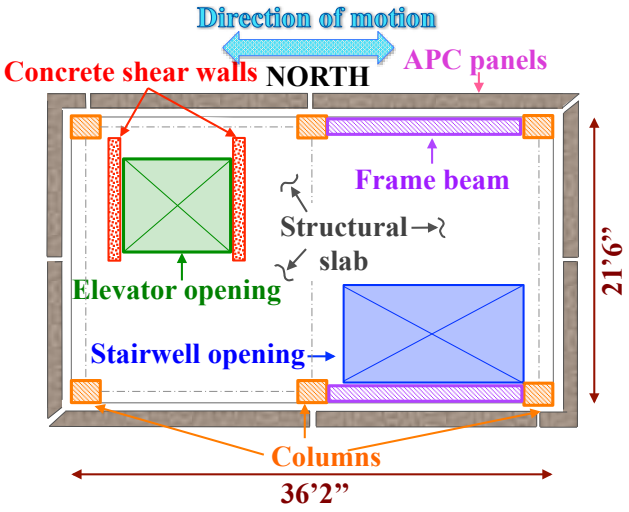


(b)

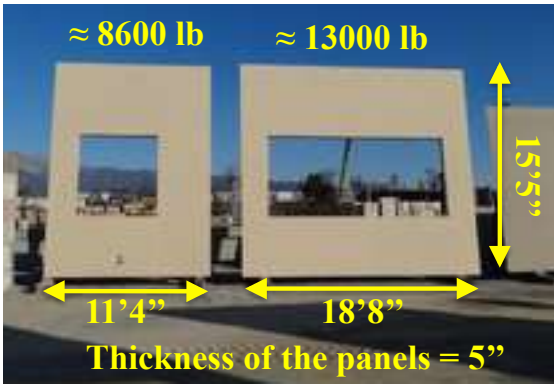


(c)

**Figure 2.7. General views of the BNCS building specimen: (a) photograph of the North and West sides of the building, (b) plan view of a typical floor, and (c) images of the APC panels during fabrication at the precast plant.**

**Table 2.1. Summary of rod lengths tested during the BNCS experiment (*d* = rod diameter, $L_f$ = free length – see Figures 3.1 and 3.2)**

| Type of connection | Short rod | | Medium rod | | Long rod | |
|---|---|---|---|---|---|---|
| | $L_f$ (inch) | $L_f/d$ | $L_f$ (inch) | $L_f/d$ | $L_f$ (inch) | $L_f/d$ |
| Sliding | snug | - | 2.9 | 3.8 | 6.4 | 8.5 |
| Flexing | 10.9 | 14.5 | 14.9 | 19.8 | 18.9 | 25.2 |

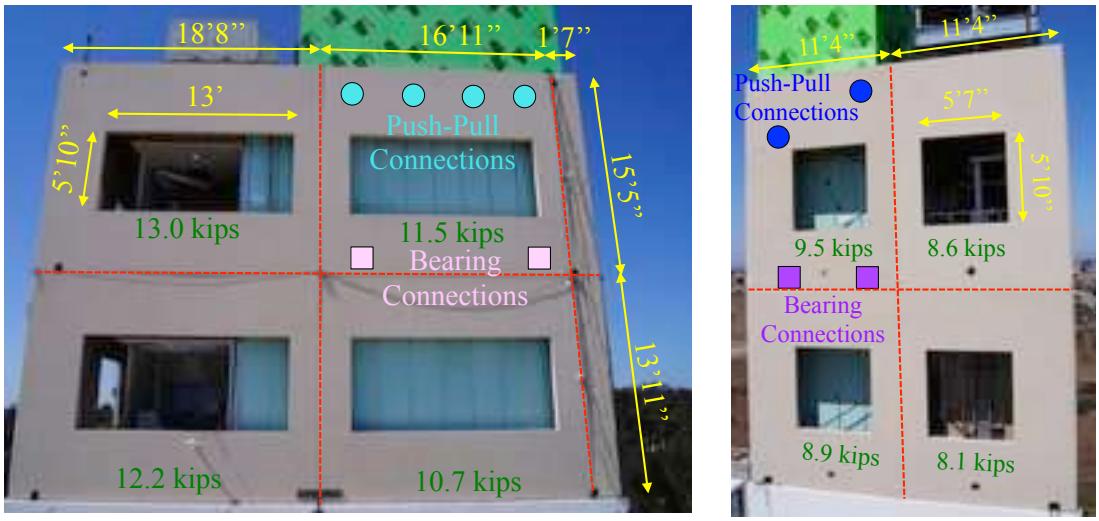


**(a)** **(b)**

**Figure 2.8. View of the APC panels installed in the BNCS building, showing the geometry and the typical location of the connections: (a) IP panels on the south side and (b) OP panels on the east side**

After each test, the panels and connections were inspected. Some of the connections displayed permanent bending of the steel (plastic bending of the connecting rods or the plate used in the connection with a ductile fuse). No damage to any of the welded connections or rod fracture was observed. The panels manifested some visible surface cracking (Cr), tearing of caulking (Ca), or permanent misalignments (Pm) precipitated by plastic bending of connection rods or plates. Video footage from cameras positioned on the roof of the structure showed the corner panels colliding under the higher drift events. A summary of the performance of the fourth and fifth floor connections and panels and corresponding peak interstory drift ratios

(PIDRs), peak interstory drifts (PIDs)[1] and peak floor accelerations (PFAs) can be found in Table 2.2 and 2.3. Performance of the APC cladding is classified based on the damage observed, for example, *none*, *minor* if mostly aesthetic, *moderate* if it requires some repair and *severe* if it is life threatening. It is important to note that when moderate *damage* to the rods in the connections were observed – although repair, by replacing the rods may be desirable – in all cases the rods still served their intended purposes, that is to continue to carry load following the test. In these tables, it is indicate the motions after which the rods were replaced. The rods were replaced after test FB3 in preparation for a larger magnitude fixed-base test, where it was desired to have elastic rods at the beginning of the test. It should also be noted that permanent misalignments and damage to joint caulking were observed through exterior inspections that could not be performed after each motion due to time constrains.

*Performance of Sliding and Flexing Rod Connections*

For both sliding and flexing rod connections *moderate* damage corresponded to a visible plastic bending of the rod post-test. As can be seen in Table 2.2 and 2.3, sliding connections with long rods did not behave as well as shorter rod configurations (Figure 2.9a), while sliding connections with medium length rods were only damaged during one motion. Some of the permanent deformations resulting in the long sliding rod connections were larger than the realized peak displacement of the connection, indicating a "ratcheting effect" where the connection binds in one direction only and slides in the other, thus accumulating residual deformations after multiple cycles.

[1] It is noted that within the present document, absent this section, the relative floor to floor drift magnitude is referred to as *story drift* to be consistent with ASCE 7-10 (2010). The terminology interstory drift is adopted in this section to be consistent with prior publications of the authors on this test series.

**Table 2.2. Performance of the APC cladding in the BNCS building - Level 4. Note that N/A ( = not available) denotes cases situations where inspections were not performed, therefore the performance level is not available.**

| Test | PIDR 4th level (%) | PID 4th level (in) | PFA 4th floor (g) | Connections | | | | | Panels | | |
|---|---|---|---|---|---|---|---|---|---|---|---|
| | | | | IP | | | | OP | Pm | Ca | Cr |
| | | | | Flexing | | Sliding | | | | | |
| | | | | medium | long | short | long | | | | |
| BI7 | 0.15 | 0.25 | 0.24 | None | None | None | None | None | None | None | None |
| FB1 | 0.24 | 0.40 | 0.31 | None | None | None | Mod.[2] | None | None | None | Minor |
| FB2 | 0.26 | 0.44 | 0.32 | None | None | None | Mod. | None | None | None | Minor |
| FB3 | 0.43 | 0.72 | 0.43 | None[1] | None[1] | None[1] | Mod.[1,2] | Minor | None | None | Minor |
| FB4 | 0.74 | 1.24 | 0.50 | None | None | None | Mod. | Minor | None | None | Minor |
| FB5 | 1.09 | 1.83 | 0.70 | Mod. | None | None | Mod. | Minor | N/A | N/A | Minor |
| FB6 | 1.29 | 2.17 | 0.65 | Mod. | Mod. | None | Mod. | Mod. | Mod. | Mod. | Mod. |

[1]Connection rod replaced to provide fresh rods for subsequent tests

[2]Connection rod replaced due to significant plastic rotation

Note: Mod.=Moderate; IP=In-Plane; OP=Out-of-plane; Pm=Permanent misalignments; Ca=Caulking; Cr=Cracking

**Table 2.3. Performance of the APC cladding in the BNCS building - Level 5. Note that N/A ( = not available) denotes cases situations where inspections were not performed, therefore the performance level is not available.**

| Test | PIDR 5th level (%) | PID 5th level (in) | PFA 5th floor (g) | Connections | | | | | Panels | | |
|---|---|---|---|---|---|---|---|---|---|---|---|
| | | | | IP | | | | OP | Pm | Ca | Cr |
| | | | | Flexing | | Sliding | | | | | |
| | | | | short | medium | short | medium | | | | |
| BI7 | 0.09 | 0.15 | 0.24 | None | None | None | None | None | None | None | None |
| FB1 | 0.13 | 0.22 | 0.35 | None | None | None | None[1] | None | None | None | Minor |
| FB2 | 0.14 | 0.23 | 0.35 | None | None | None | None | None | None | None | Minor |
| FB3 | 0.23 | 0.38 | 0.47 | None[1] | None[1] | None[1] | None[1] | None | None | None | Minor |
| FB4 | 0.36 | 0.60 | 0.57 | None | None | None | Mod. | None | None | None | Minor |
| FB5 | 0.54 | 0.90 | 0.68 | None | None | None | None | None | N/A | N/A | Minor |
| FB6 | 0.66 | 1.11 | 0.65 | None | Mod. | None | None | None | None | Minor | Minor |

[1]Connection rod replaced to provide fresh rods for subsequent tests

Note: Mod.=Moderate; IP=In-Plane; OP=Out-of-plane; Pm=Permanent misalignments; Ca=Caulking; Cr=Cracking

Snug sliding connections behaved well as expected, with no damage observed. In general, flexing rod connections showed better performance than sliding connections. In fact, connections with long and medium rods showed yielding only during the final tests FB-5 and FB-6. Figure 2.9b shown the typical deformation observed in the case of flexing connection, which tend to create hinge at the two edges. The short flexing connections installed at the fifth level did not show any permanent bending throughout the entire test sequence. These observations led also to the conclusion that for both types of connections the actual working mechanism includes both sliding and bending (Pantoli et al., 2013c).

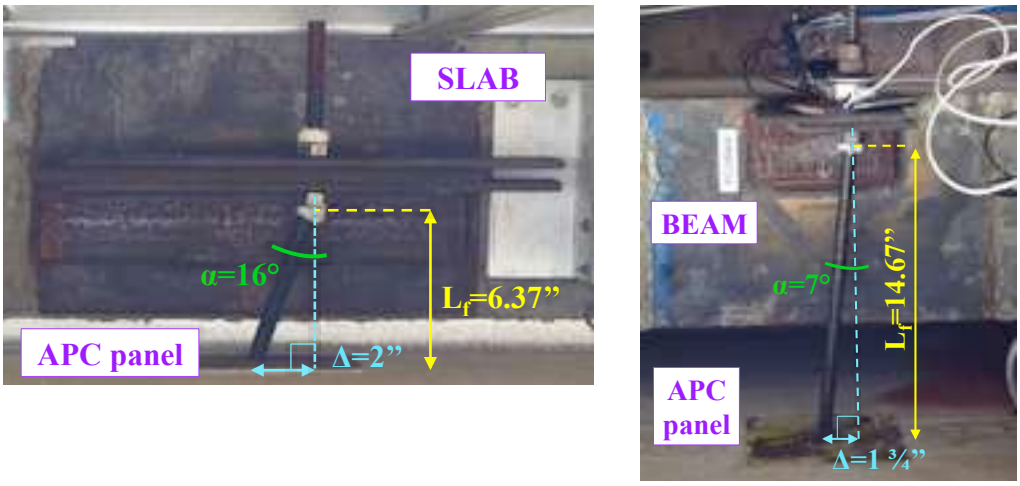


**Figure 2.9. Example of performance of connections: (a) long sliding rod after FB3, and (b) medium length flexing rod after FB5. Views looking up at connection.**

*Permanent Misalignment, Damage to Caulking and Cracking of the Panels*

After the final motion, the upper portions of both the southern and northern (OP) panels on the west side of the fourth level observed a permanent westward misalignment with respect to the bottom of the panels on the fifth level. The final position of the upper portion of the northern panel (the one with butt return joint) was ~1.6in west of its original position while the southern panel (having a miter joint) had a permanent westward misalignment of ~0.6in. Long sections of

caulking tore off completely at the fourth floor and fifth levels after FB-6. Examples of these type of damage can be observed in Figure 2.10. This permanent misalignment was the expected result of the ductile fuse corner connection, which yields in bending when the panels contact each other. Minor cracking of the panels started from the first BI motions but was very limited and cracks were generally small (~0.004in). Cracking reached a moderate level only at few locations after the final motion at the fourth level.

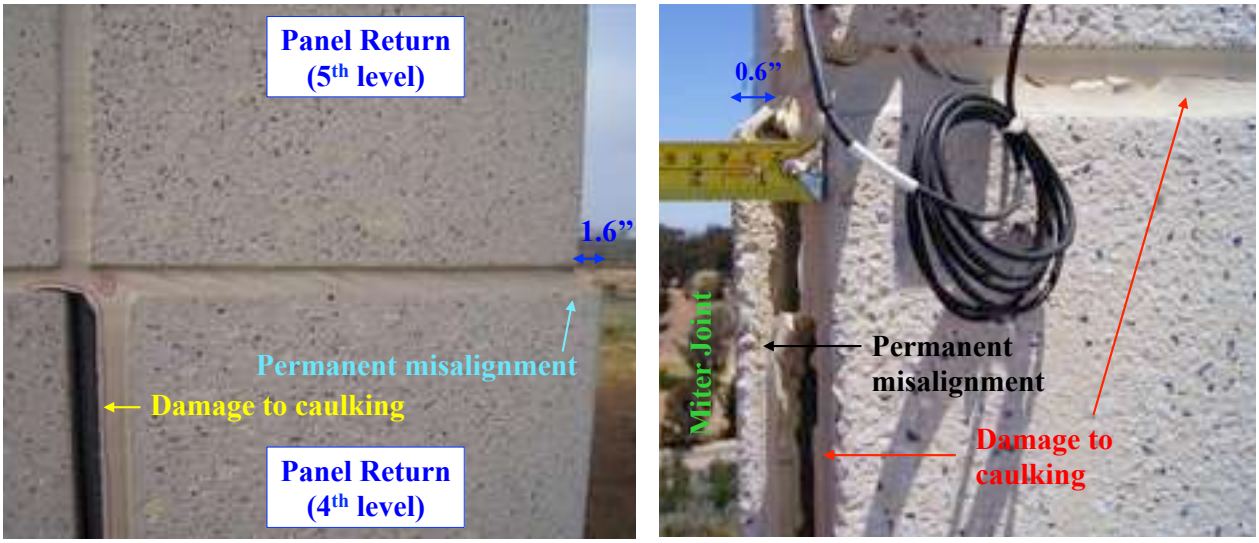


(a) (b)

**Figure 2.10. Damage to caulking and permanent misalignment observed after FB6 for a (a) northwest corner with butt return joint, (b) southwest corner with miter joint.**

*Measured Results – Acceleration Amplification*

Four panels (two OP and two IP) were instrumented with accelerometers to capture response in the direction of input motion imposed by the shake table. These measurements were used to calculate the amplification of the acceleration in the panels with respect to the building. In these analyses, the uncorrelated acceleration amplification factor is calculated as the ratio of the maximum Eastward (or Westward) acceleration in the panel to the maximum Eastward (or Westward) acceleration in the slab. Figure 2.11a and c show the peak acceleration measured in

the slab connected to the bottom of the panel versus the peak panel acceleration during the six FB motions. In this case, it can be observed that all measurements can be bound by the linear 1:1 and 2:1, i.e. the amplification factor is between 1 and 2. Figure 2.11b and d shows the same plot but considering the accelerations in the slab connected to the top of the panel. In this case the acceleration amplification factors vary from roughly 0.9 (i.e., the peak acceleration in the panel is smaller than that in the slab) to 1.6.

These analyses indicate the mean of the distribution is 1.28 and 1.1 for the top and bottom slab, respectively. Measurements of the top slab show that in all cases the accelerations amplified, with some reaching a maximum of 2.0 (or double that of the slab); whereas 90% of the accelerations compared with the bottom slab were amplified. These plots clearly show that the peak accelerations in the panels are generally greater than those at the floors in which they are connected, and in some case the amplification is considerable. In the current design approach, connections are designed for a force related to the expected acceleration in the building, absent consideration of the impact of the potential for dynamic modification due to the panel itself. Considering the present results, and assuming a 90th percentile, an amplification of bottom and top floor peak accelerations of 1.6 and 1.3, is observed. These test results suggest the actual amplification of forces may be higher than code estimates for precast panel connections in the lower range of floor accelerations. It is important to note however, that since the design case accelerations were not achieved, it is not clear that this amplification would hold true for upper bound floor acceleration cases.

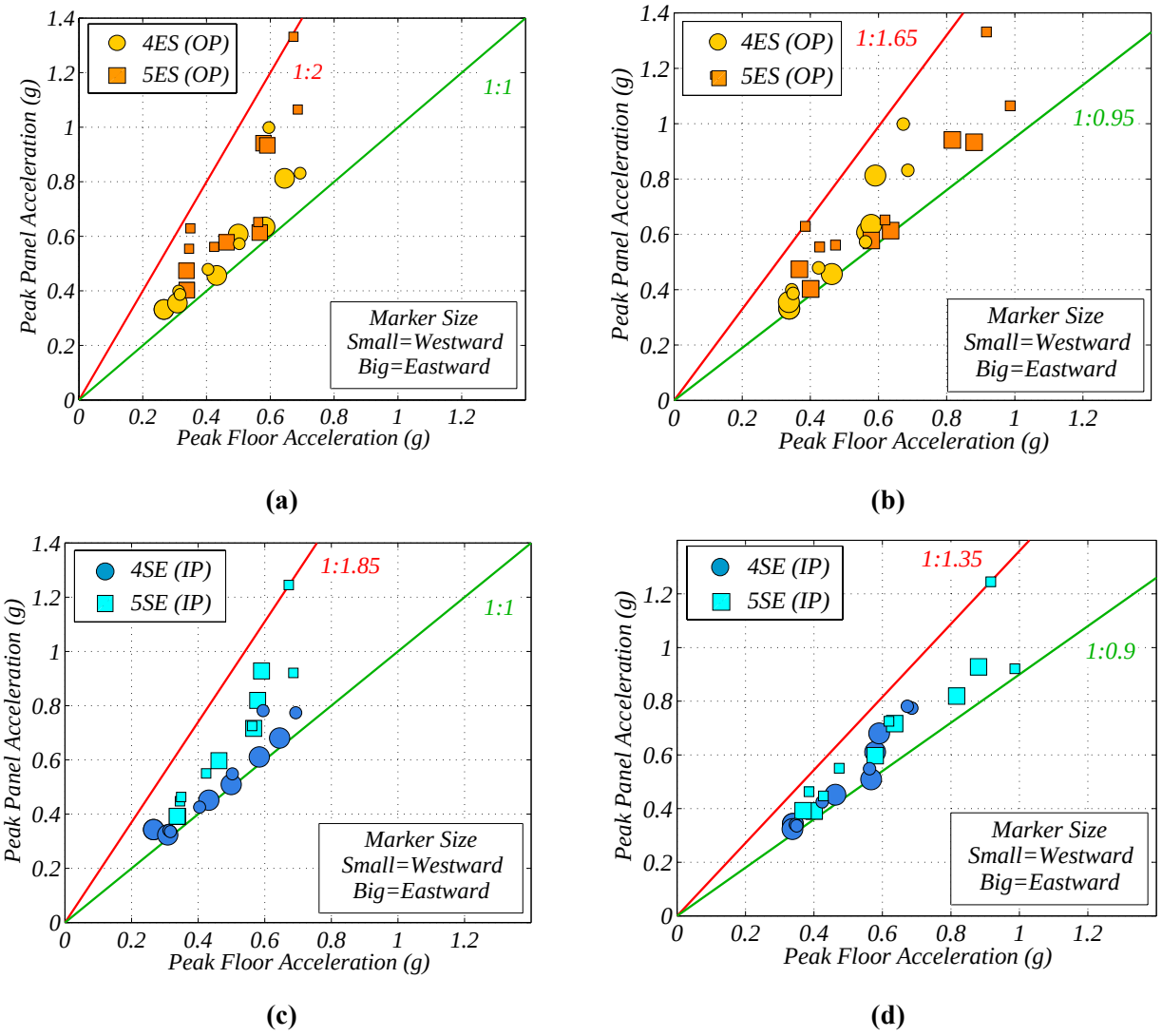


**Figure 2.11. Acceleration amplification within the APC panels in the BNCS tests: (a) and (b) peak floor acceleration versus peak panel acceleration in the OP panels respect to bottom and top slab, (c) and (d) peak floor acceleration versus peak panel acceleration in the IP panels respect to bottom and top slab.**

*Response of Corner Connections*

The current state of practice is to oversize the relevant panel joints to prevent panel collisions at the corners of the building during a large seismic event, but this may result in an unappealing reveal on the building exterior. For this reason, in the BNCS test program a new connection with a ductile fuse allowing for smaller corner joints was explored and installed at each corner

connection. In this new corner system the floor-to-floor relative displacements are (ideally) absorbed as follows:

- *Elastic drifts* are absorbed by the closing of the vertical corner joint, with the joint sized sufficiently to avoid impact; and
- *Inelastic drifts* are larger than the vertical corner joint and therefore intended to result in impact of the joint. However, upon impact the ductile fuse is designed to prevent connection overload through the fuse mechanism, ensuring that the panels remain attached to the building after the event. In this work, the ductile fuse was in the form of a cantilevering bending plate that deformed during impact. At the same time, it was sized to avoid damage to the other parts of the panel/connection. A picture of this connection is shown in Figure 2.12a. A schematic of the corner system during inelastic drift demands for the southeast corner is shown in Figure 2.12b and c.

The actual behavior of the corner joints in the southwest and northwest corners of the building was captured during testing by video cameras. Screenshots showing the opening and closing of the vertical joint during FB6 for the butt return and miter are shown in Figure 2.13 and 2.15 respectively. These video were taken from a camera fixed to the roof slab and hence this is the point of reference. It is noted also that all the panels were cast straight, and the apparent curvature of the OP panel in Figure 2.13 is a distortion created by the camera. Further information about the behavior of the corners can be found in Pantoli et al. 2013d.

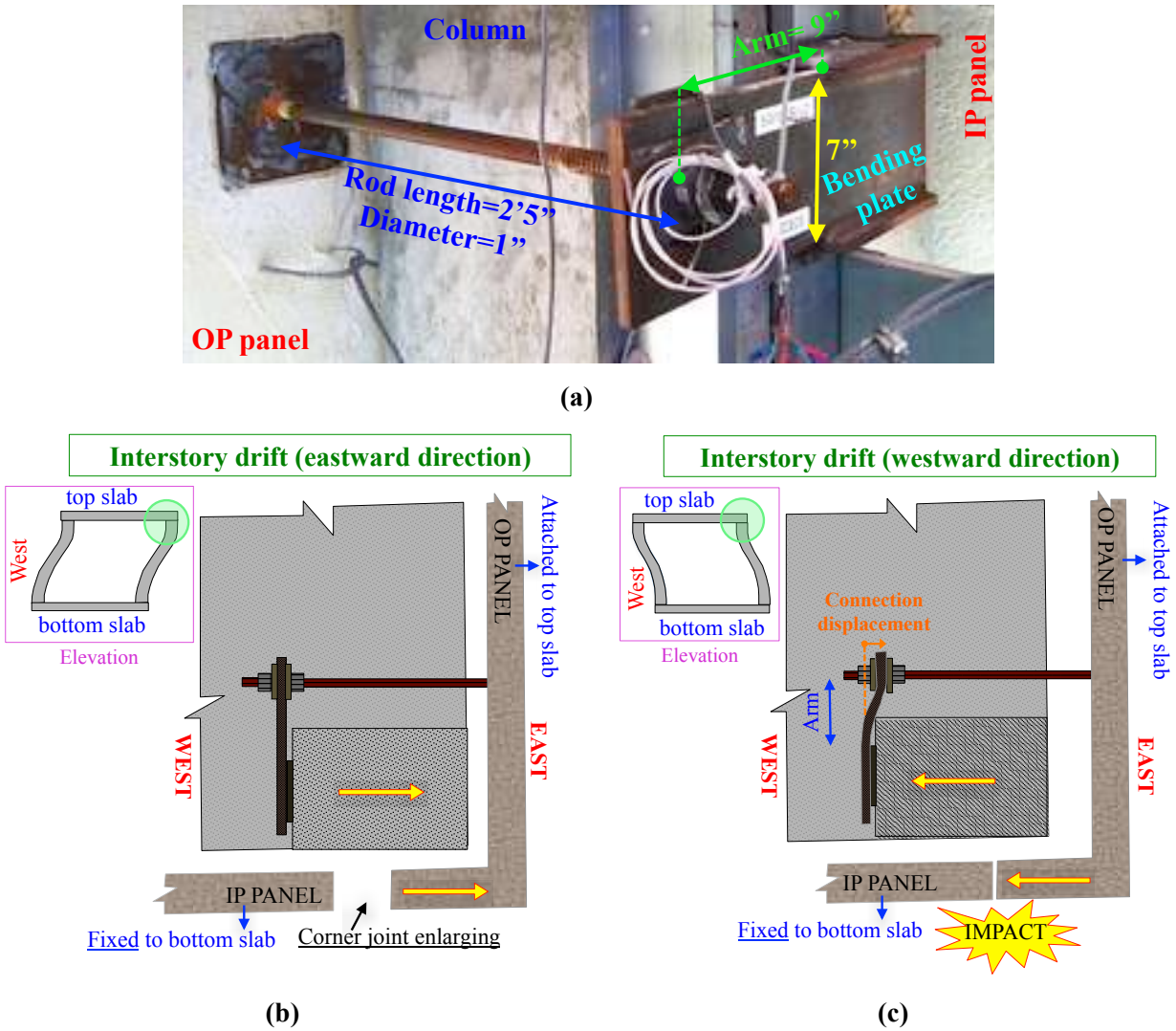


**Figure 2.12. Push-pull corner connection with ductile fuse on the OP panels (a) photograph, (b), (c) conceptual schematic showing the desire behavior of a corner connection in the 4ES panel during Eastward and Westward motion. Note: the circle in the elevation schematic of parts b and c denotes the corner considered in the respective plan views; yellow arrow denotes direction of movement of OP panel and top of column.**

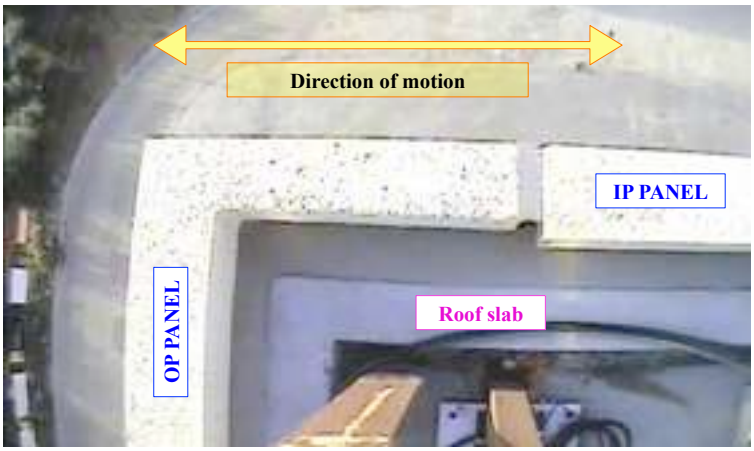


**(a)**

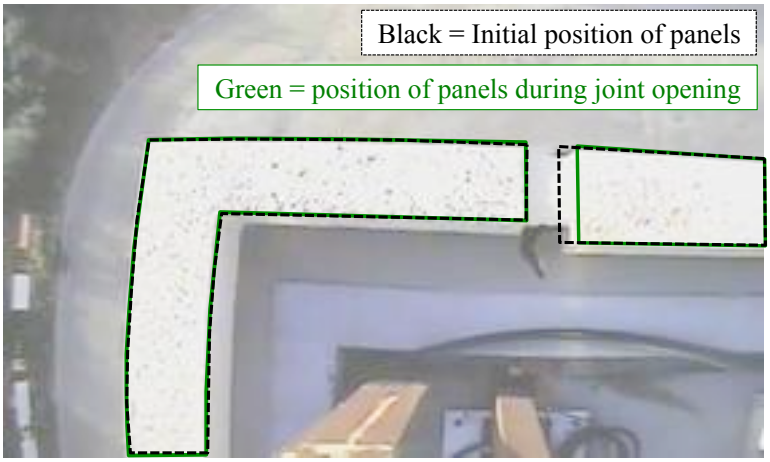


**(b)**

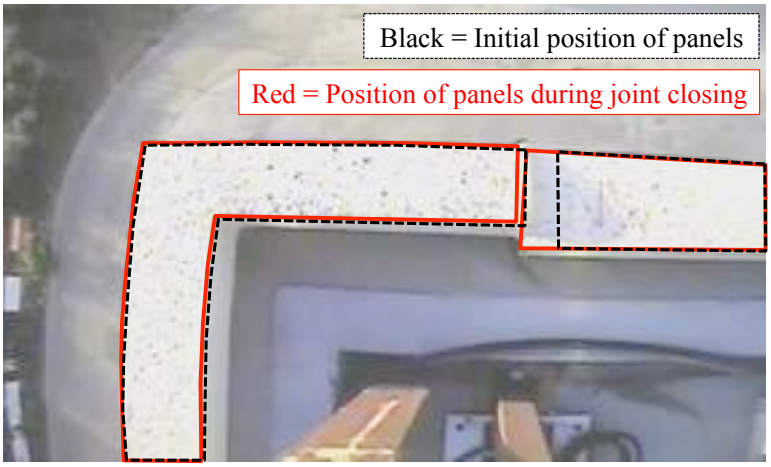


**(c)**

**Figure 2.13. Screenshots from videos of the corner joints view from the roof during FB-6 for the butt-return joint in the NW corner showing (a) original position, (b) joint opening and (c) joint opening (view looking down)**

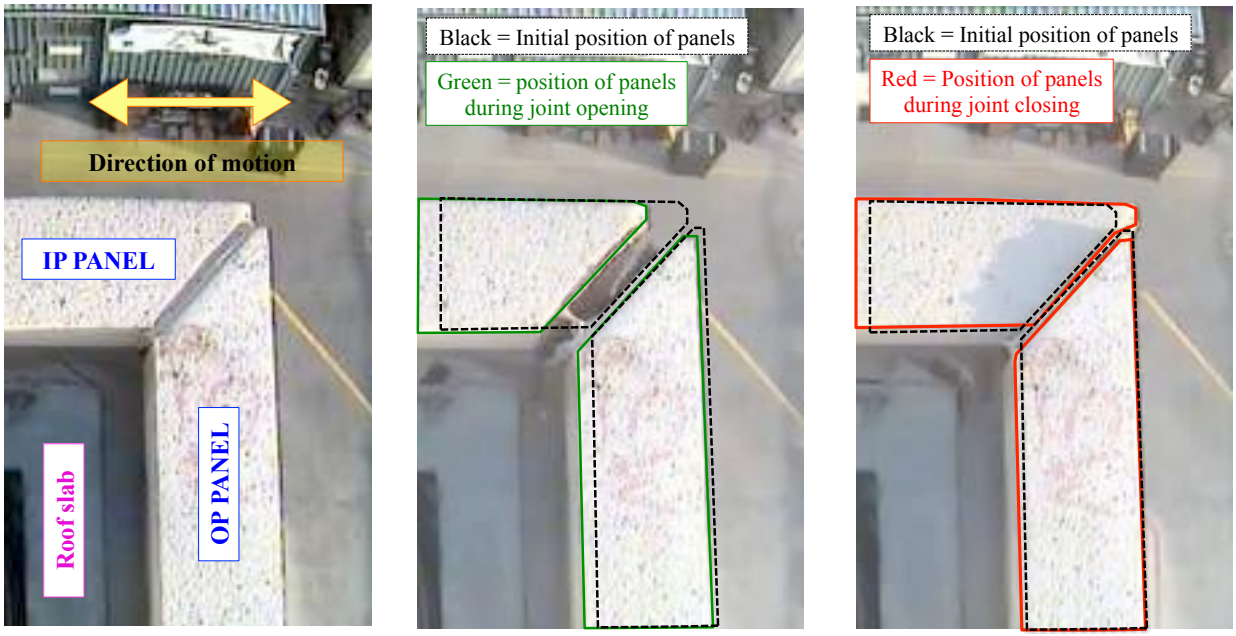


**(a)** **(b)** **(c)**

**Figure 2.14. Screenshots from videos of the corner joints view from the roof (view looking down) during FB-6 for the miter joint in the SW corner showing (a) original position, (b) joint opening and (c) joint closing**

The observed damage to the corner areas of the panels revealed that the performance of the newly developed corner connection with ductile fuse was dependent on the type of corner joint. In fact, while in the panels with butt-return joints the plastic bending of the ductile plate was activated and the corner area on the panels remained uncracked, the OP panels with miter joint cracked close to the corner connection embed and the plastic bending of the plate was not activated. This difference in behavior is clearly shown also by the histeretical response of the connections, which display the hardening behavior typical of steel in the case of a connection with butt return joint and a softening or linear response for the connections close to miter joints. Hysteresis loops recorded during FB6 in connections close to miter and butt-return joints is shown in Figure 2.15a and b respectively. It is possible to conclude that the presence of a butt-

return gives stiffness to the corner thus reducing flexural distortion in the panel and forcing the ductile fuse in the connections to absorb the deformation.

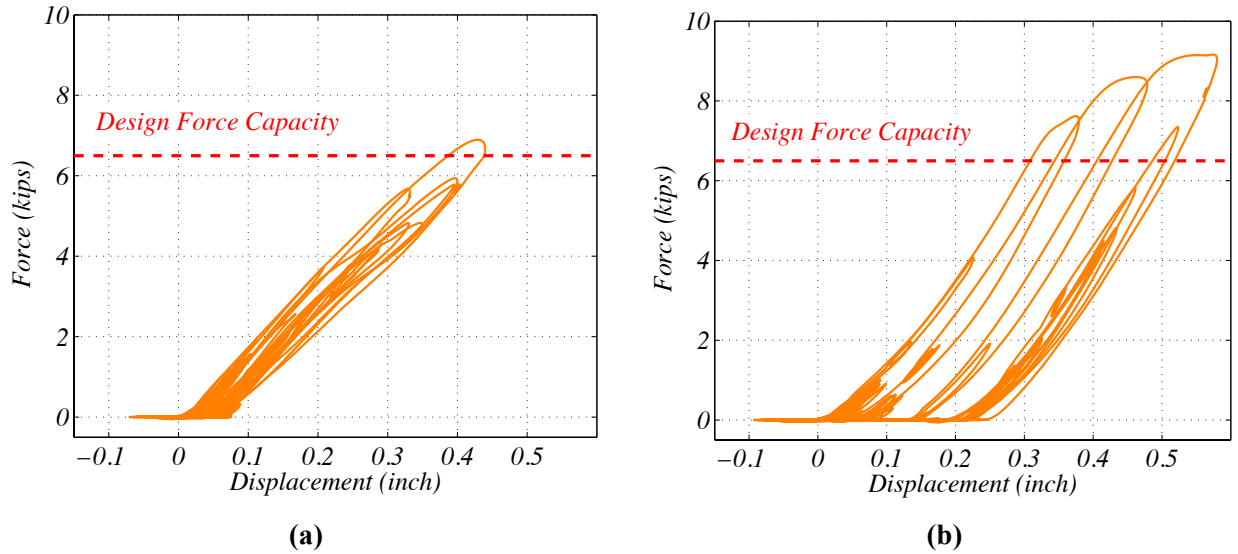


**Figure 2.15. Hysteretic behavior of the push pull connection during FB6 for a corner connection close to (a) a miter joint, and (b), a butt return joint.**

### 2.2.2 Component-Level Studies: Flexing Connections

In parallel with the BNCS test program, a suite of flexing rod component tests were conducted at San Jose State University (McMullin, 2014). The goal of the flexing connection component tests was to experimentally determine the failure limit for flexural loading of a coil rod connection. Tests provided cyclical force-deformation data for connections with varying length and diameter of rods as well as cycles of loading prior to failure. A primary goal of the testing was to determine the number of cycles resisted by the coil rod as a function of the lateral deformation applied. A series of 16 experiments were performed using the test configuration shown in Figure 2.16. All rods were commercially available coil rod of either ¾-inch or 1-inch diameter, ASTM A36 Grade. Mill certifications for the ¾'' rods indicated an average yield and ultimate stress of 48.6 and 71.4 ksi, respectively; and an elongation at fracture ranging from 22 to 27%, for the 3/4" diameter rod. Additional information reguarding the material properties of the rods used in

this test are provided in Appendix A. Free rod lengths varied from 10.9 to 18.9 inches. Rods were loaded either with cycles of constant displacement or cycles of incrementally increasing amplitude. Experiments were concluded when the rod could no longer support an axial load of approximately 300 pounds.

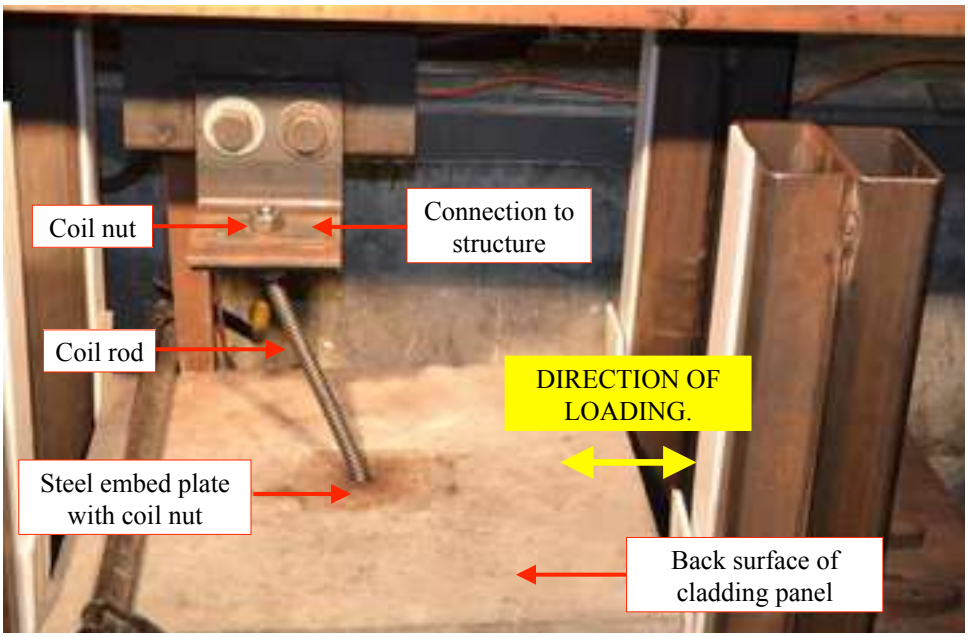


**Figure 2.16. Experimental set-up for flexing connection component tests**

All connections failed due to fracture of the rod in the inelastic region. Inelastic hinging could be observed concentrating at both ends of the rod. During the tests, instrumentation recorded the lateral force applied to the rod and the relative displacement of the two ends of the rod. Figure 2.17 is a plot of one representative component experiment and the corresponding behavior of a flexing connection from the BNCS experiments. For the graph, the data has been normalized by the maximum force recorded. In Figure 2.17 the component tests are shown in red and the data from the BNCS experiments are shown in blue. Most component-test specimens have a bilinear response for the first excursion of loading, reaching the peak force in this first excursion. The unloading and reloading then follows a response curve consistent of most low-

carbon steel materials. Trailing cycles of loading did see modest decrease in the maximum force resisted. The data for the BNCS tests are developed by using relative displacements of the rods recorded during the experiment. Since load cells are not available for the horizontal forces on the rods during the BNCS tests, the normalized force is calculated just normalizing the acceleration measured on the panels.

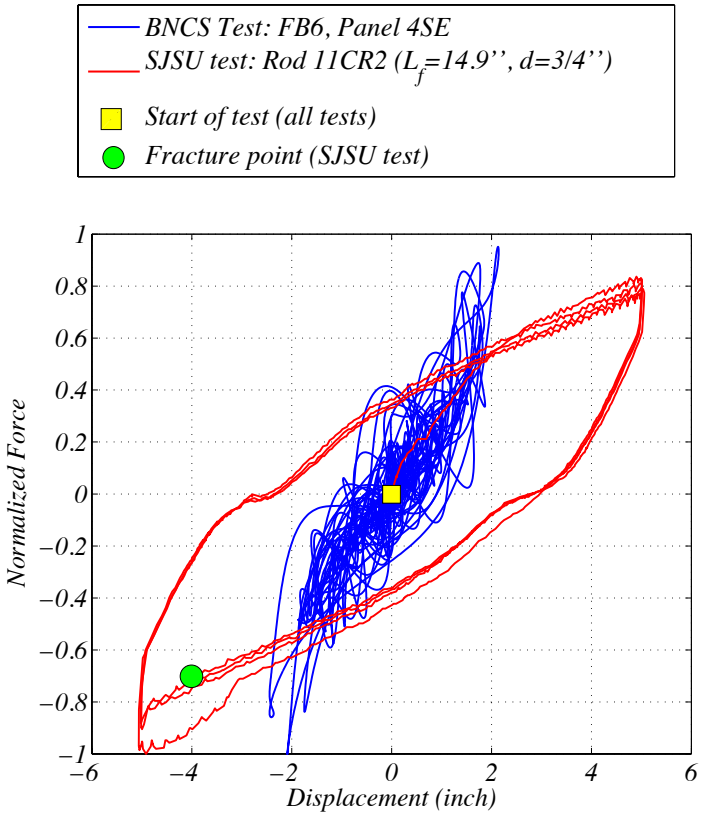


**Figure 2.17. Normalized force-displacement response for a rod with $L_f$ = 14.9 inch and d=3/4 inch coil rod during a SJSU test and a normalized acceleration-displacement response for a IP panel during the BNCS experiment**

Figure 2.18 shows a summary of the results from the BNCS (system) and SJSU (component) tests in terms of damage observed for the different rod lengths. In both plots, the y-axis shows the total number of cycles creating a displacement in the rod larger than the theoretical yield displacement calculated considering the rod hinging at both ends. For the SJSU tests, this

corresponds to the total number of cycles, while for the BNCS experiment the number of cycles was calculated using the rainflow counting algorithm, a commonly adopted method in fatigue calculations. The x-axis of the plot shows the average rotation angle for all cycles in which the displacement exceeded the theoretical yielding displacement. The two datasets are binned first by limit state achieved (Figure 2.18a) and subsequently by L/d ratio (Figure 2.18b). In these plots, $L$ is taken as the free length ($L_f$ in Figure 3.1 and 3.2). It is noted that rods achieving fracture carried far fewer theoretical plastic excursions, but to very large rotations (red stars). It is also important to note that no apparent trend is evident when analyzing these data with regard to $L_f/d$. Figure 2.19 further presents these data as a function of $L_f/d$ (part a) and $(L_f/d)/D_{pI}$ (part b). In this case $D_{pI}$ is the story drift ratio, using the notation of ASCE 7-10. Results are shown for those rods that suffered fracture during the SJSU component tests. Linear regression demonstrate the poor data fit when relating to $L_f/d$ (coefficient of determination $r^2 = 0.44$); whereas by incorporating the displacement, a much more reasonable fit is achieved ($r^2 = 0.86$).

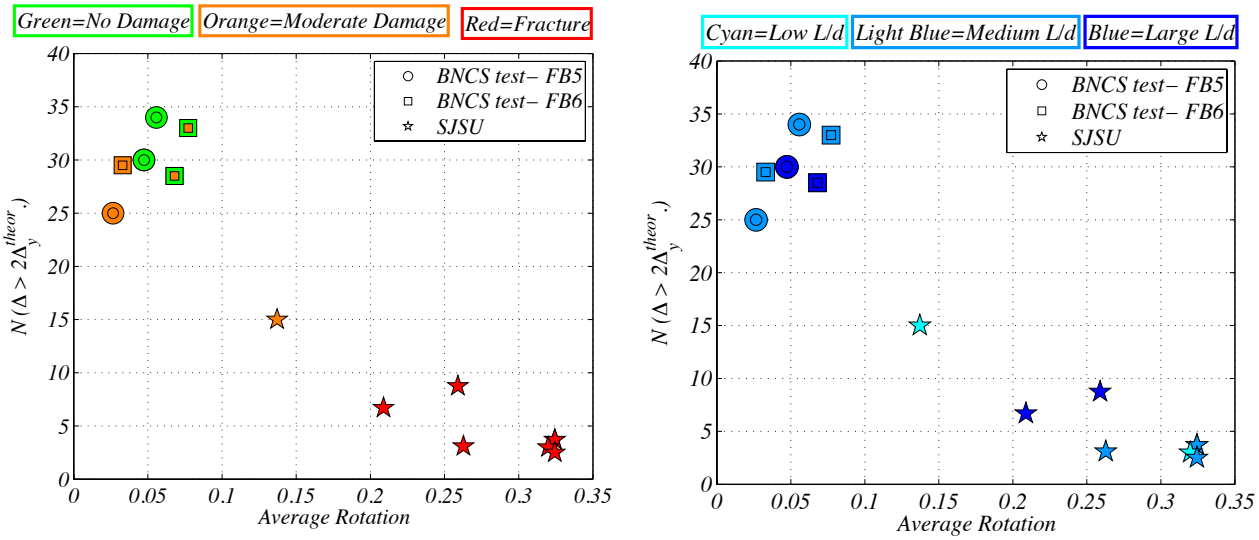


**(a)** **(b)**

**Figure 2.18. Number of cycles with a peak-to-peak displacement greater than twice the theoretical yield displacement versus average rotation of the connection: (a) binned by limit state and (b) binned by $L_f/d$ ratio. (BNCS system tests and SJSU component test data)**

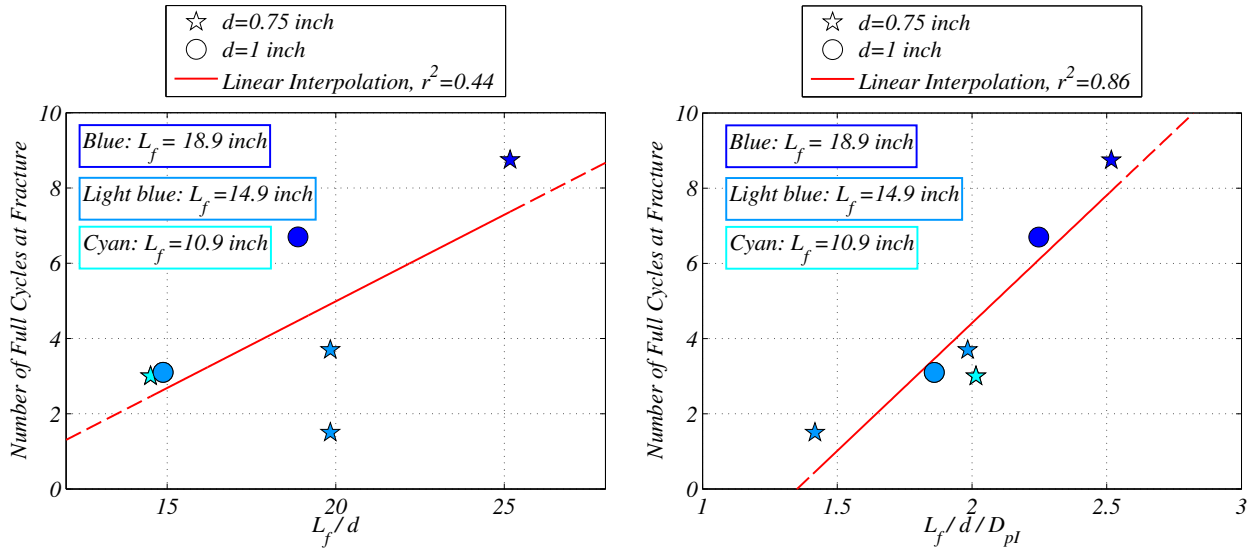


**Figure 2.19 Number of cycles to fracture (SJSU component data only): (a) versus L/d and (b) versus (L/d)/$D_{pI}$. Note: $D_{pI}$ in this case in the imposed drift during testing**

Several observations were made related to the behavior of the flexing rod, particularly when the results were combined with the experimental data collected during the BNCS experiments.

1. Rods with free lengths of 14.9 inches or longer are able to accommodate deflections of 5.0 inch or more.
2. The ability to resist several cycles of high displacement is related to the prior load history. Rods that were tested by initially applying small displacements and then continued with many cycles of increasing displacement were unable to resist as many cycles of large displacement.
3. The number of cycles of constant rotation of the plastic hinges of the rod appears to be inversely related to the applied rotation. The limit appears to be independent of rod diameter as the ¾-in and 1-in rods tested showed comparable number of cycles prior to failure. As would be expected, if the rods are not loaded past their yield displacement, they should be able to accommodate a significant number of cycles of loading.

4. The inelastic region of the rods as observed during fracture was over a short length, approximately one to two diameters of the rod. If the rods were loaded in pure tension the inelastic region may be expected to extend nearly the full free length of the rod. The relatively localized yielding may be due to multiple reasons, including the large moments developed at the ends of the rods, the geometric complexity of the threads, and the effect of cold-working of the steel. However, even though the inelastic region of the rod was small, the rods did resist several cycles of inelastic loading and resisted displacements far above the yield displacement, indicating good ductility of the material.

### 2.2.3 Component-Level Studies: Sliding Connections

The widespread use of sliding connections by precasters, the lack of code specifics regarding their design, and the poor performance of long rod sliding connections observed in the BNCS test by the authors motivated execution of a component test program specifically on sliding connections (Pantoli et al., 2014b). These dynamic component tests were conducted on a pair of sliding connections supporting a model mass, which in turn was loaded using a single axis shake table for seismic input with the configuration shown in Figure 2.20.

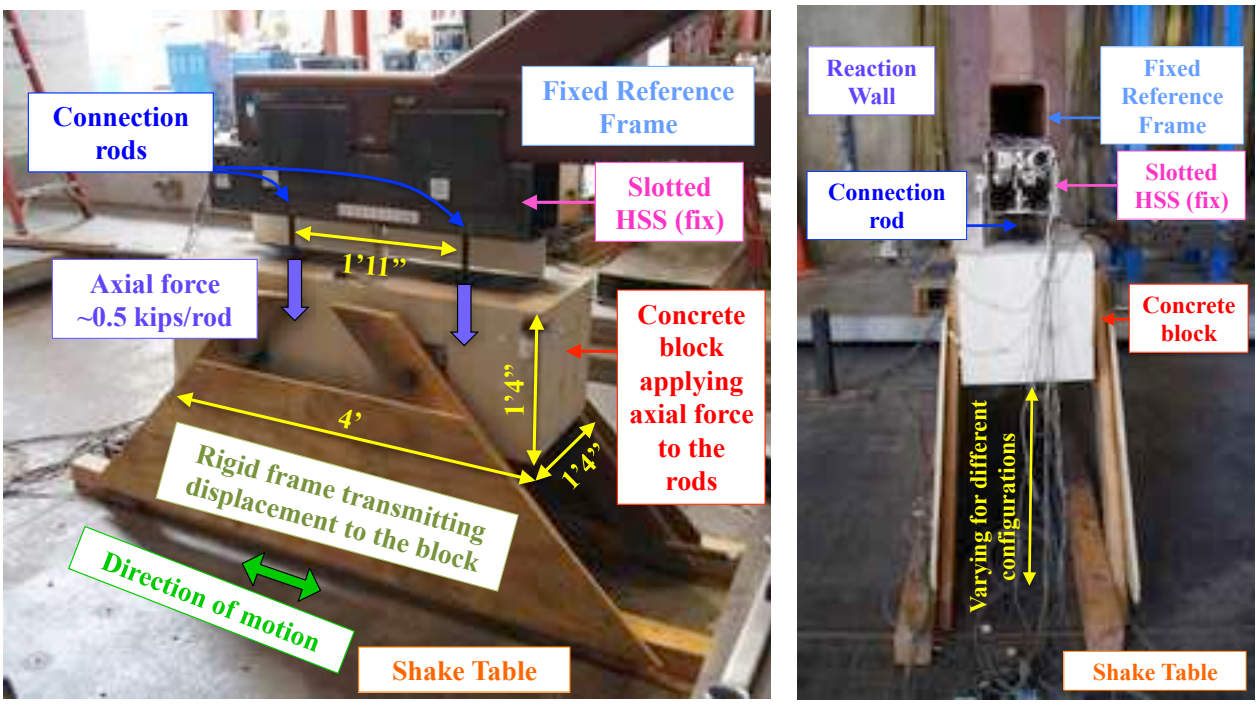


(a) (b)

**Figure 2.20. Component test setup (a) side view, and (b) end view**

The goal of these tests was to evaluate the influence of different parameters on the performance of sliding connections, whose typical configuration is shown in Figure 2.21a. It is noted that early on in the test program, the compression plate washer was eliminated since it was observed to cause binding of the rods. In total, six different configurations characterized by different rod lengths and diameters were tested. This coil rod was of ASTM A36 Grade and included diameters of ¾" and 1". Tension tests on the ¾'' and the 1'' diameter rods were performed. For the ¾'' diameter the average $f_y$ was 59.6 ksi the average $f_u$ was 72.5 ksi, while elongation varied from 16 to 19%. For the 1'' diameter rods the average $f_y$ was 58.6 ksi, the average $f_u$ was 79.2 ksi and the elongation varied from 24 to 26%. The damage state observed for each of the five motions run (denoted as M1-M5) in each configuration are summarized in Figure 2.21b.

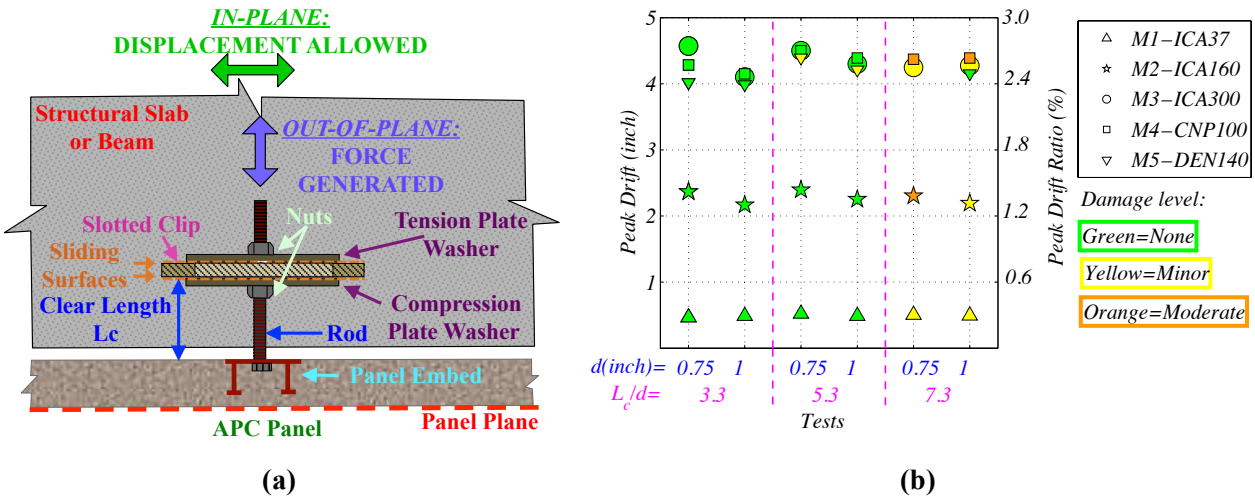


**Figure 2.21. (a) Schematic plan view of a sliding connection, and (b) results of the component tests. Note that the peak drift ratio is provided for reference only and is estimated assuming a floor-floor height of 14 feet**

The following practical outcomes emerge these tests:

- Sliding rod connections with nuts and washers on both sides of the slotted element tend to respond in a *binding* mode instead of *sliding*. Due to the flexibility of this connection, the rod bends prior to the activation of the intended sliding motion. Indeed, the frictional resistance depends on the frictional coefficient between the sliding surfaces and the normal force applied to the surface, both of which have a large variability, particularly during dynamic loading, as occurs during seismic motion. If the bending-induced rotations are large enough, a clamping force is created between the sliding plates and the slotted angle, which makes sliding less likely. This can occur even when relatively short, stiff rods are used. These connections can also exhibit ratcheting behavior, accumulating deformations in one direction, while sliding in the other direction. Therefore, connection rods that are designed to slide but instead deform in a bending mode can reach high rotations at

low drift magnitudes. It is possible that severe damage – in the form of fracture of the rods - would occur if the imposed displacements reach large values.

- As a result, several modifications are needed to improve the performance of sliding connections. For example, the free rod length can be removed, in such cases a bolt may be more readily utilized. Snug sliding connections consistently demonstrated good performance (as demonstrated in the BNCS system-level test). Alternatively (or in addition), the compression plate washer can be removed. The elimination of this plate washer makes it impossible for the clamping force to develop. Sliding connections without the compression plate washer responded with a well-defined sliding mechanism for all $L_c/d$ ratios tested. However, due to the permanent plastic rotations required to initiate sliding it is recommended that the $L_c/d$ ratio be limited to 5.3. It is noted that removing the compression plate washer obviously makes the connection a tension connection only. Compression loads will have to be resisted by some other mechanism or connection – such as a push only connection separate from the tension rod. Precasters have achieved this by welding an angle clip to the structure that rests against the back of the panel after it has been aligned.

# 3 PRINCIPLES OF DESIGN

The primary goal of designing the connections of a precast cladding system is to provide a load path to the structure for all forces acting on the cladding panels. In addition, the precast panel system must be designed to accommodate both lateral and vertical movements of the building primary structural system. Due to the rigidity of these panels, improperly designed connections may result in their inadvertent participation within the vertical or lateral load path of the primary structure. As a result, the cladding panels may restrain the structure as it moves in response to applied loads – clearly an undesirable outcome. The designer therefore must either allow for ample movement of the panel relative to the building, or design for the consequences of impact and load transfer. In what follows, the principles of designing APC systems to either 1) accommodate large relative displacements or 2) allow impact during seismic displacements are synthesized. This discussion is drawn from the knowledge of current code provisions, balanced by the findings of the aforementioned test programs, and harmonized with current practice. Prior to discussing these issues however, the importance of accommodating forces to the APC system is first discussed.

## 3.1 ACCOMODATION OF SEISMIC FORCES

The APC panel and its connections must be proportioned to resist seismic inertial forces per ASCE 7, Sections 13.3.1 and 13.5.3 (d), with amplification factor, $a_p$, and response factors, $R_p$, for body elements and fastener elements as stipulated in 13.5.3 (d). Seismic forces are combined with dead load effects to produce the most critical combination of forces.

$$F_p = \frac{0.4 a_p S_{DS} W_p}{\left(\frac{R_p}{I_p}\right)}\left(1 + 2\frac{z}{h}\right) \qquad \text{(ASCE 7, Equation 13.3-1)}$$

It should be noted that the values of $a_p$ and $R_p$ stipulated in Table 13.5-1 of ASCE 7 provide a much amplified force for fastener components of connections, in an effort to prevent brittle failure modes. The higher force level is intended to maintain the response of these elements in their elastic range. Also, this amplified force level satisfies the exception to the ductility provisions of D3.3.4.3d and D3.3.5.3c of ACI (2011) Appendix D for anchorage to concrete.

## 3.2 ACCOMODATION OF RELATIVE DISPLACEMENT

### 3.2.1 Design of Sliding Connections

A typical sliding connection consists of an embed in the panel, a bolt (in particular for snug connections) or a threaded connecting rod (¾" or 1" diameter), a slotted clip welded to the structure, and plate washers and nuts. The threaded rod is connected to the APC panel via a threaded insert attached to the panel embed. It then extends through the slotted clip and is sandwiched by plate washers and nuts (Figure 3.1a-b). The nuts must be no more than finger tight to minimize binding and should be prevented from loosening. Sliding connections are intended to allow relative in-plane movement between the panel and building by allowing the threaded rod to slide inside the slotted clip (Figure 3.1c). The rod transmits out of plane forces through axial tension and compression to the embed and the plate washers, but is free to slide in-plane, thus isolating the panel from story drift. The slot length is determined by adding two times the story drift plus the rod diameter and erection tolerance (which is usually 1") – see for example Figure 3.1b. One challenge with sliding connections during building movement is that even though the nuts are only finger tightened, friction between the washers and connection can impose a bending force on the rod. As the rod rotates, the nuts and washers bind and prevent sliding. Research has shown that sliding connections with longer more flexible rods have an increased tendency to bind (see for example Chapter 2 – Section 2.2.3). A key provision of good

sliding performance is to reduce the clear length (Figure 3.1b) of the rod. Research outlined in Chapter 2 supports a maximum Clear Length/Rod diameter ratio ($L_c/d$) of 5.3. It is important to note, however, that the optimum performing sliding configuration incorporates a snug assembly, with the compression washer removed (Chapter 2 – Section 2.2.3).

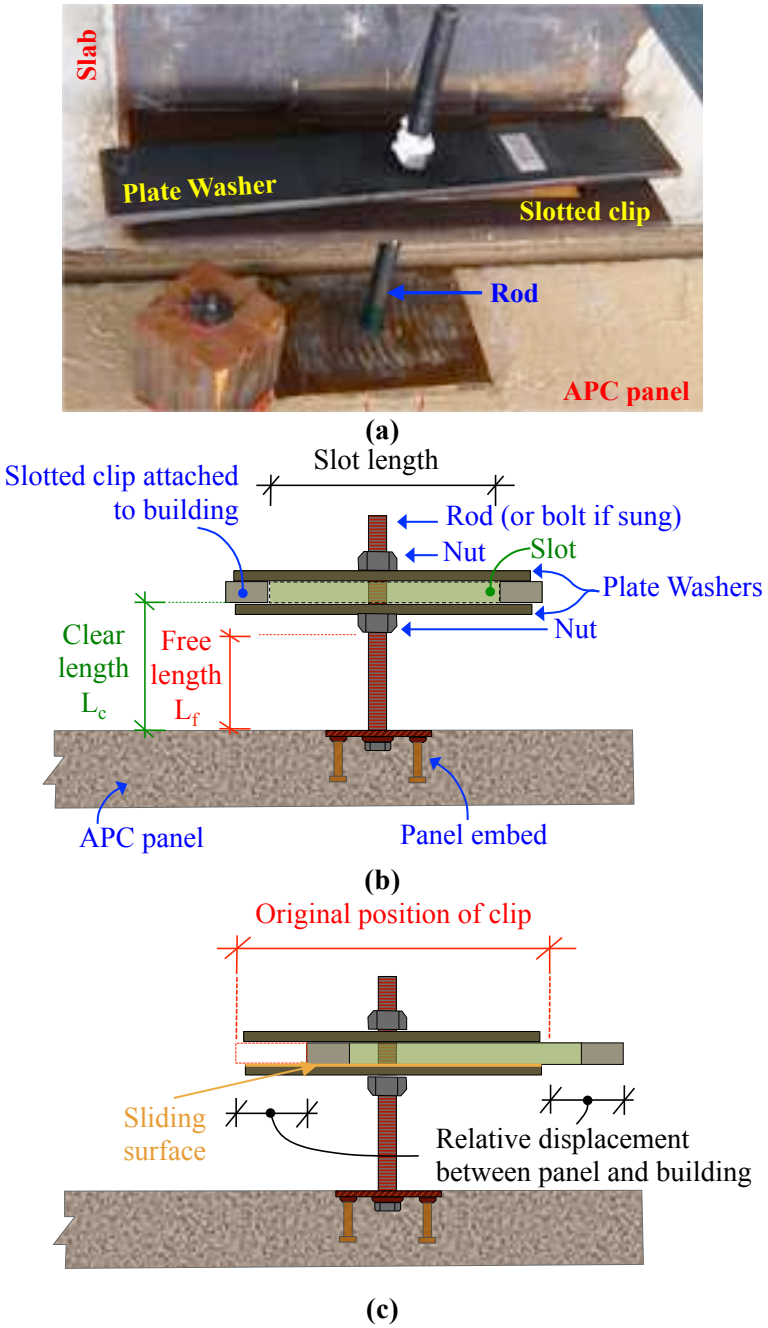


**Figure 3.1. Sliding connections: (a) photograph, (b) and (c) schematic of original configuration and intended behavior during building movement.**

### 3.2.2 Design of Flexing Connections

A typical flexing rod connection involves similar components as used in sliding connection, however the rod is longer and the through hole in the clip is oversized only to account for installation tolerance (Figure 3.2a-b). Flexing rod connections allow relative displacement through bending behavior of a relatively long threaded rod connecting the panel to the building (Figure 3.2c). This bending is accommodated by a combination of elastic and inelastic behavior in the rod. The length of the rod is a primary design variable; if it is too short cyclic loading may lead to failure of the rod. Coil threaded rods are often preferred by precasters because of the convenience of the large thread profile. They thread quickly, rarely bind or strip, and provide a reliable connection. However, care must be taken in specifying coil threaded rods. Much of the use of coil threaded rods is for applications much different than flexing such as concrete forming and temporary construction operations, and the rod manufacturers provide high strength rods optimized for axial tension. The high strength rods are usually a higher carbon material that is non-ductile in flexure. For this reason, it is important to specify the coil threaded rod be manufactured from a base material known to be ductile such as ASTM A36. Research has shown that rod free length, diameter, and story drift are key variables in good flexing rod connection performance. The research outlined in Chapter 2 supports a miminum free length/diameter/story drift $(L_f/d)/D_{pI}$ of 6.0.

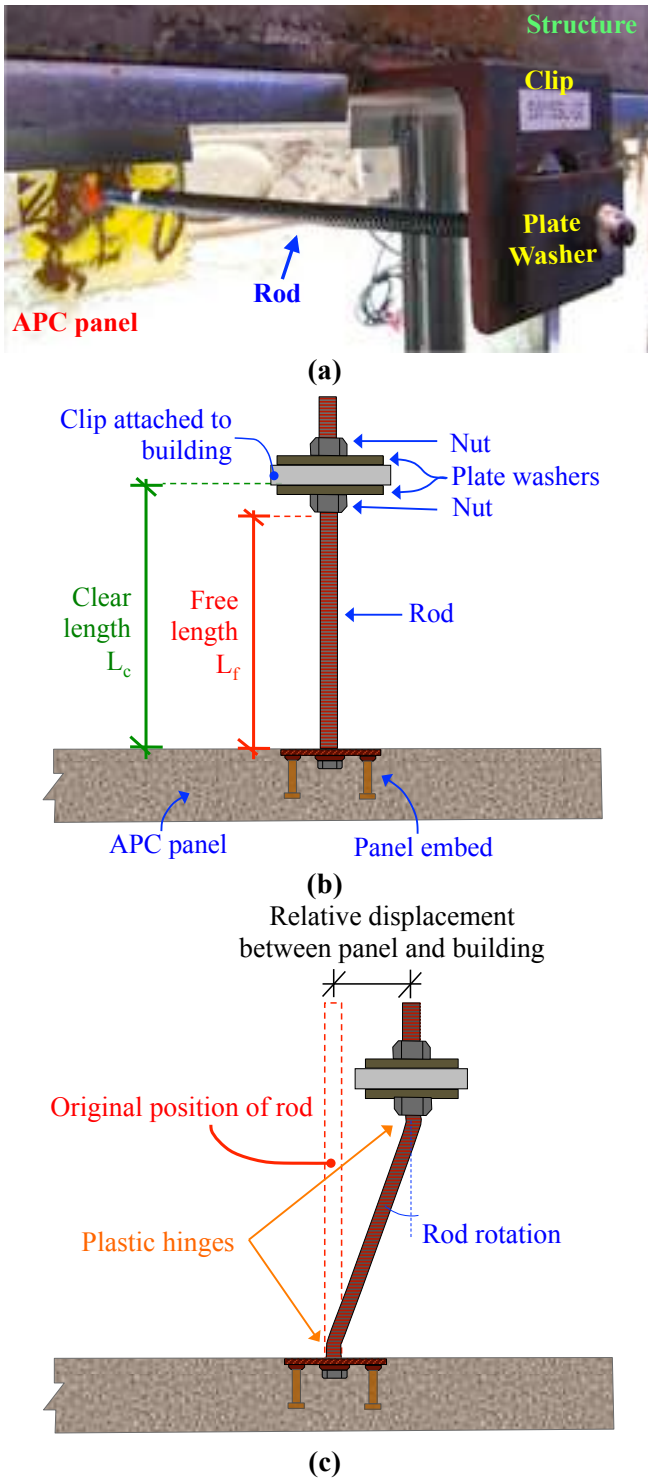


**Figure 3.2. Flexing connections: (a) photograph, (b) and (c) schematic of original configuration and intended behavior during building movement.**

## 3.3 ACCOMODATING DRIFTS AT CORNER JOINTS

The corner joints of APC panels constitute a particularly critical location in the system because this is the point where the in-plane (IP) panels and out-of-plane (OP) panels meet. Ideally, the IP panels move rigidly with the lower slab, while the top of the OP panels are attached to and move with the upper slab (Figure 2.13). The relative motion of the tops of the two panels meeting at the corner is essentially the same as the relative motion of the upper and lower floors. The current state of practice is to oversize the relevant panel joints to prevent panel collisions at the corners of the building during a large seismic event as per ASCE 7 Section 13.5.3 (a):

*"Connections and panel joints shall allow for the story drift caused by relative seismic displacements ($D_p$) determined in Section 13.3.2, or 0.5 in. (13mm), whichever is greatest"*

The parameter $D_p$ is calculated using inelastic drift values $\delta x = C_d \, \delta_{xe}$ from Section 12.8.6. Alternatively, if elastic analysis of structure is unavailable, $D_p$ may be determined from code limits on story drift $\Delta_a$ from table 12.12-1. In contrast to adopting the calculated inelastic drift values when sizing the seismic joint, it is suggested that a ductile connection will support reduction of the joint size. The following design example presents a corner system for conventional and ductile design philosophies.

## 3.4 DESIGN EXAMPLE

In what follows, all of the design procedures for typical APC push-pull connections are presented, while adding the unique design aspects that apply to corner situations. In a conventional design, the size of the vertical joint allows the corner panels to move the maximum code prescribed story drift without colliding. In contrast, to achieve a ductile design, here it is proposed that the vertical joint size is reduced and large inelastic story drift is accommodated by

yielding of one of the connection components. In the present design, this component is called a *ductile fuse*.

To demonstrate the design of a corner joint considering these two philosophies, a panel is assumed to be installed between the 4th and the 5th floor (corresponding to the roof) of a 5-story reinforced concrete special moment frame office building[1]. The design spectral response acceleration at short periods $S_{DS}$ is 1.0, the importance factor of the building $I_p$ is 1.0 and the story height h is assumed to be 13'. The geometry of the panel is presented in Figure 3.3. The panel and its return are 5-inch thick and the concrete has a uniaxial compressive strength $f_c$' of 5000 psi. The total weight of the panel W is determined as 11.2 kips.

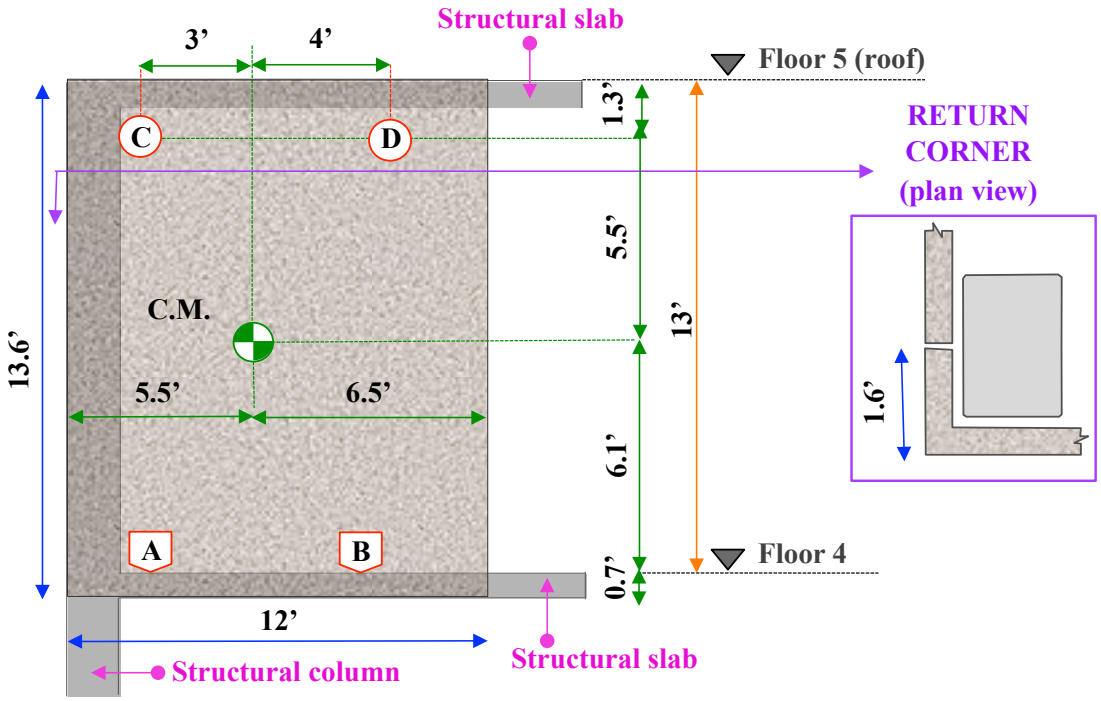


**Figure 3.3. Detailed geometry of the APC panel under consideration (left: elevation; right; plan schematic). C.M. denotes center of mass.**

[1] Unless otherwise noted, the following design codes are used in the present design example: ACI 318 (2011); ASCE 7-10 (2010 – not including Supplement 1); and AISC 341-10 (2010). For brevity they are referred to simply as ACI, ASCE-7, and AISC, respectively.

The panel is supported by two bearing connections at the bottom (A and B) and two push-pull connections at the top (C and D). The connection under consideration is the upper push-pull corner connection, denoted with the letter C. The mass tributary to connection C can be calculated by equilibrium as:

$$W_p = \left(\frac{4}{3+4}\right)\left(\frac{6.1}{6.1+5.5}\right)11.2 = 3.36\ kips$$

Figure 3.4 shows the connection configuration proposed for both design philosophies. The steel specified for the anchors, rods, and plates is ASTM A36 ($f_y$=36ksi, $f_u$=58 ksi). The 1'' diameter coil rod has an unthreaded cross-sectional area $A_b$ of 0.78 inch$^2$, a threaded cross-sectional area $A_t$ of 0.606 inch$^2$ and a threaded radius of gyration $r_t$=0.22 inch.

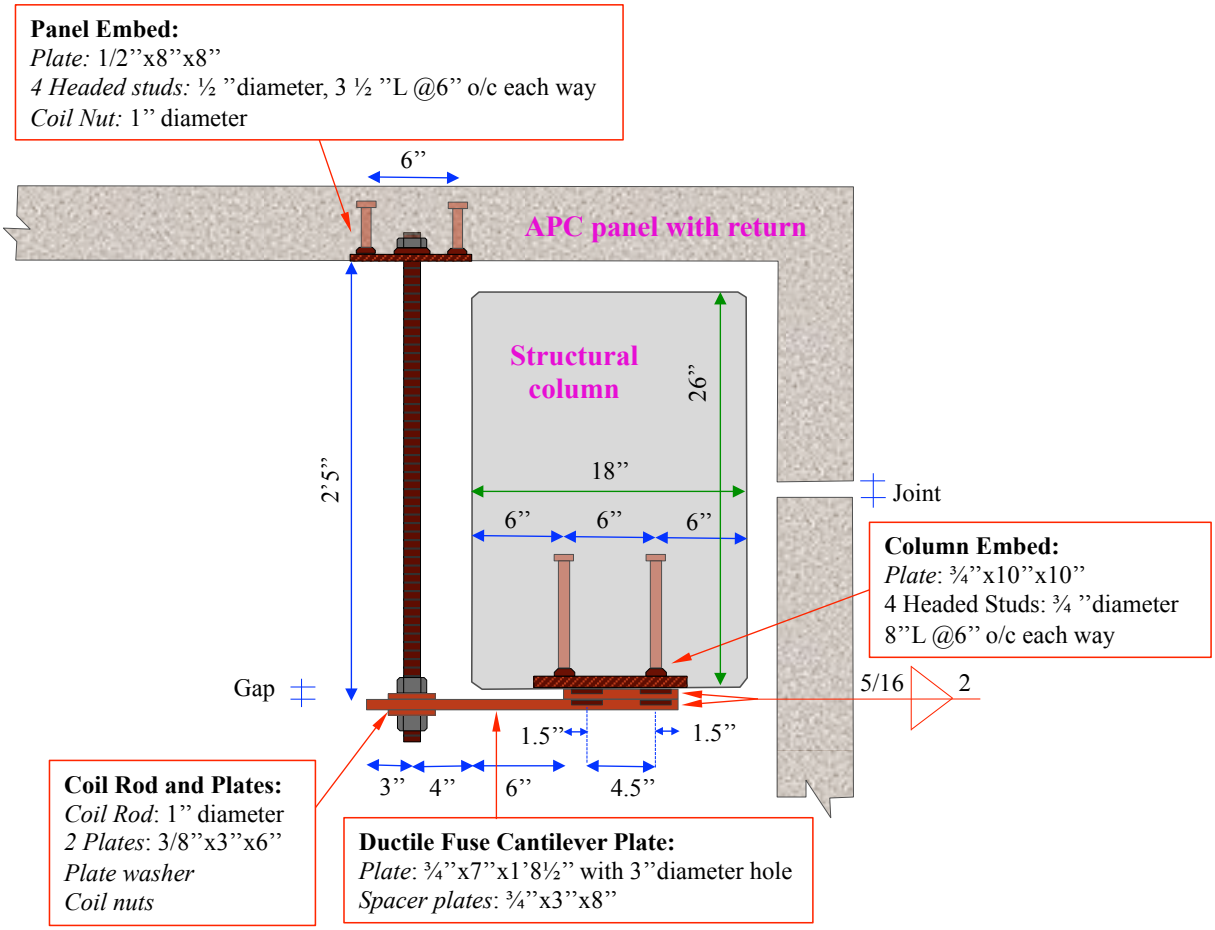


**Figure 3.4. Corner connection details (plan view)**

The connections will first be checked against inertial forces. This phase of design is the same for ductile and conventional approaches. Then, the vertical joint needs to be sized in each case. Finally, for the ductile design approach there is a final step of checking that the capacity of the ductile plate is smaller than the capacity of the other components of the connection – this will ensure that the ductile plate yields prior to its adjacent components. These three steps will be presented in the following sections.

### 3.4.1 Evaluating Connection Components for Inerital Forces

This first step is the same for the conventional and ductile design and it consists of determining that all connection components can withstand the design seismic inertial forces prescribed in ASCE 7:

$$F_p = \frac{0.4 a_p S_{DS} W_p}{\left(\frac{R_p}{I_p}\right)}\left(1 + 2\frac{z}{h}\right) \qquad \text{(ASCE 7, Equation 13.3-1)}$$

In the case under consideration the equation reduces to:

$$F_p = \frac{0.4 \cdot a_p \cdot 1 \cdot W_p}{\left(\frac{R_p}{1}\right)}(1 + 2 \cdot 1) = \frac{1.2 \cdot a_p \cdot W_p}{R_p}$$

ASCE 7 Table 13.5-1 provides amplification and reduction coefficients, $a_p$ and $R_p$, respectively, to determine the component response to the earthquake motions. For exterior nonstructural wall panels, there is a tiered force system whereby connections have more stringent design parameters to account for force magnification due to the component response, and amplification of forces to account for non-ductile behavior of connections. The resulting coefficients for design of the panel itself and the body of connectors is $a_p$ = 1.0 and $R_p$ = 2.5, while for the fasteners of the connection $a_p$ = 1.25 and $R_{p,}$= 1.0. The body of a connector would

be a sub-element in the connection that fails in a predictable or ductile mechanism, like yielding of plates or rebar. A fastener would be a sub-element of the connection that fails in a brittle manner such as fracture of a weld or bolt, or breakout of a concrete shear cone. This leads to the following value of forces for the body and fasteners of the connection:

$F_{p,body} = 0.48W_p$

$F_{p,fastener} = 1.50W_p$

In this example, the above values do fall within the bounds of the code minimum and maximum limits for $F_p$ noted below:

$F_{p,min} = 0.3S_{DS}I_pW_p = 0.3W_p$ (ASCE 7, Equation 13.3-2)

$F_{p,max} = 1.6S_{DS}I_pW_p = 1.6W_p$ (ASCE 7, Equation 13.3-3)

Figure 3.5 shows a numbered diagram of all the components of the connection in the load path, and Table 3.1 annotates whether the component qualifies as a body or fastener of the connecting system, and the corresponding design force level.

The final value of $F_{p,body}$ and $F_{p,fastener}$ for connection C can be calculated considering that $W_p$ for this connection is 3.36 kips.

$F_{p,body} = 0.48 \cdot 3.36 = 1.61$ kips

$F_{p,fastener} = 1.50 \cdot 3.36 = 5.04$ kips

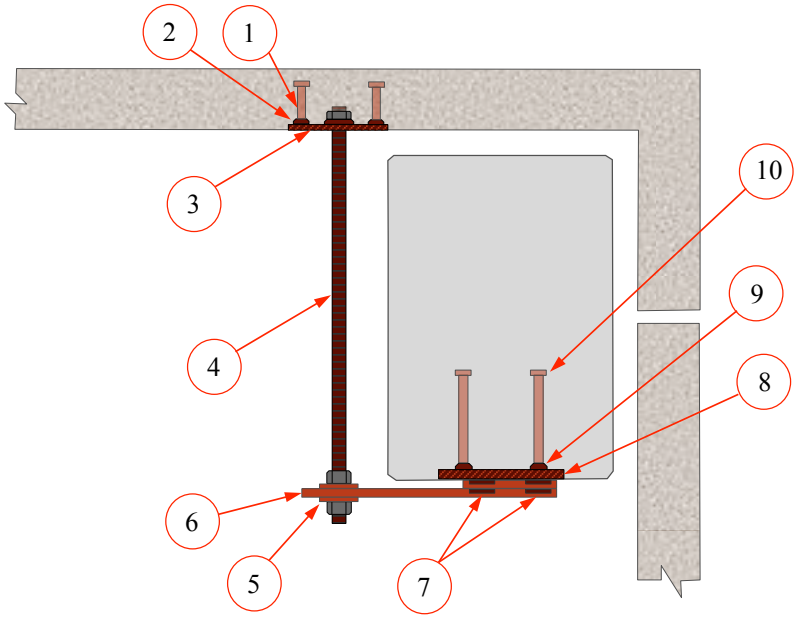


**Figure 3.5. Components of the corner connection (refer to Table 3.1 for nomenclature)**

**Table 3.1. Components of the corner connections per Figure 3.5**

| Component # | Component Name | Type | $F_p$ |
|---|---|---|---|
| 1 | Headed Stud | Fastener | 1.50 $W_p$ |
| 2 | Stud Weld | Fastener | 1.50 $W_p$ |
| 3 | Embed Plate | Body | 0.48 $W_p$ |
| 4 | Threaded Rod | Fastener | 1.50 $W_p$ |
| 5 | Plate Washer | Body | 0.48 $W_p$ |
| 6 | Cantilever plate (*ductile fuse*) | Body | 0.48 $W_p$ |
| 7 | Plate Welds | Fastener | 1.50 $W_p$ |
| 8 | Embed Plate | Body | 0.48 $W_p$ |
| 9 | Stud Welds | Fastener | 1.50 $W_p$ |
| 10 | Headed Stud | Fastener | 1.50 $W_p$ |

***Component #1 - Headed Studs in the Panel Embed (Fastener)***

The headed studs need to be checked aginst two types of failure: the breakout of concrete and the failure of the steel. The detailed characteristics of the panel embed are shown in Figure 3.6.

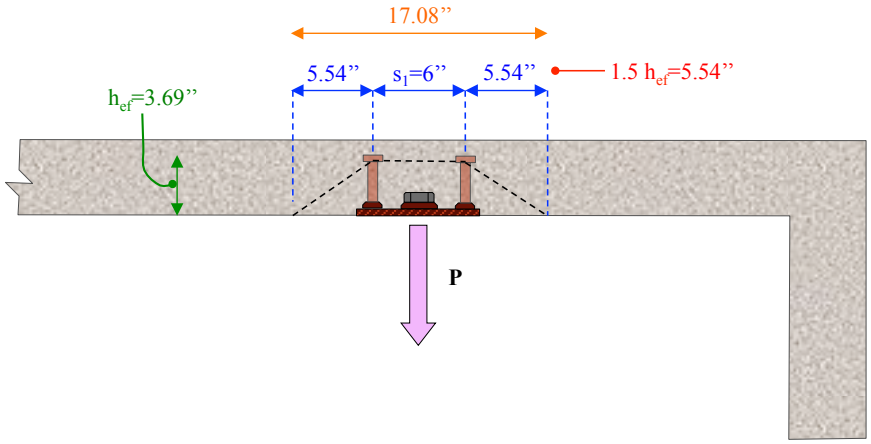


**Figure 3.6. Detail of the panel embed**

*Concrete Breakout*

Design against concrete breakout is performed following the prescriptions found in ACI-Appendix D and using the following quantities:

- The effective embedment depth of the anchors $h_{ef}$ = plate thickness + stud length – head thickness = (0.5” + 3.5” – 0.313” = 3.69”).
- The breakout surface is defined as a square whose sides are equal to the inter-anchor space $s_1$ plus two times $1.5h_{ef}$ (ACI, Fig. RD.5.2.1);
- The modification factors for eccentric load $\Psi_{ec}$, edge effects $\Psi_{ed}$, cracking $\Psi_c$ and for post-installed anchors $\Psi_{cp}$ are all equal to 1. Their definition can be found in ACI sections D.5.2.4 – D.5.2.7.
- The anchor is cast-in, thus the parameter $k_c$ is equal to 24 (ACI, Equation D-7);
- The concrete is normalweight, and the corresponding $\ell$ factor is 1.0. (ACI, Section 8.6).

The check against concrete breakout can be performed following the procedure in ACI, Section D5.2. The parameter $A_{NCO}$, which is the projected concrete failure area of a single anchor with an edge distance equal to or greater than $1.5h_{ef}$, is defined as:

$$A_{NCO} = 9h_{ef}^2 = 9 \cdot (3.69)^2 = 123\ inch^2$$ (ACI, Equation D-6)

The paramter $A_{NC}$ is the projected concrete failure area of a single anchor group (ACI, Section D.5.2.1), and in this case is:

$$A_{NC} = (s_1 + 1.5h_{ef} + 1.5h_{ef})^2 = (17.08)^2 = 292\ inch^2$$

The basic concrete breakout strength of a single anchor in tension in cracked concrete $N_b$ is defined as:

$$N_b = k_c \lambda \sqrt{f_c'} h_{ef}^{1.5} = 24\sqrt{5000}\ 3.69^{1.5} = 12.0\ kips$$ (ACI, Equation D-7)

Finally, the basic concre breakout strength of the group will be:

$$N_{cbg} = \frac{A_{Nc}}{A_{Nco}} \Psi_{ec} \Psi_{ed} \Psi_c \Psi_{cp} N_b = \frac{292}{123} \cdot 1 \cdot 1 \cdot 1 \cdot 1 \cdot 12.0 = 28.5 kips$$ (ACI, Equation D-5)

The capacity to demand relation needs to be satisfied in all cases such that:

$$\phi N_n > N_{ua}$$ (ACI, Equation D-1)

However, in Seismic Design Categories C, D, E, or F (ASCE 7), there is an additional reduction in capacity applied to concrete failures modes such that:

$$0.75\ \phi N_n > N_{ua}$$ (ACI, Section D3.3.3)

Applying the additional reduction factor of 0.75 yields:

$$0.75\ \phi N_{cbg} = 0.75 \cdot 0.75 \cdot 28.5 = 16.0\ kips > F_{p,fastener} = 5.04\ kips$$ **OK**

*Steel Anchors*

The capacity of anchors in tension can be found through ACI, Appendix D considering that the number of anchors per embed *n* is 4, the effective cross sectional area on the single anchor in tension $A_{se,N}$ is 0.2inch$^2$ and that the ultimate strengh for the anchor in tension $f_{uta}$ is 60ksi:

$N_{sa} = nA_{se,N}f_{uta} = 4 \cdot 0.2 \cdot 65 = 52\ kips$ (ACI,Equation D-3)Then:

$\phi N_{sa} = 0.75 \cdot 52 = 39 kips > F_{p,fastener} = 5.04\ kips$ **OK** (ACI, Equation D-1)

***Component #2 – Headed Stud Welds***

The headed stud welds qualify as a fastener component and have to be designed for shear through the effective throat of the fillet weld. The length of the weld is calculated based on the fracture surface of the weld, located on the the mid-thickness of the weld (Figure 3.7).

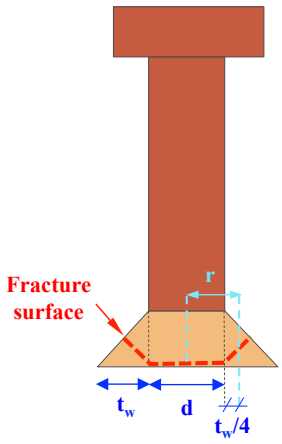


**Figure 3.7. Fracture surface of the stud welds**

In this case, L = 2πr, where r is equal to the radius of the stud plus a quarter of the thickness of the weld (Figure 3.7).

$L = 2\pi\left(0.25 + \frac{0.313}{4}\right)$=2.06''

The weld capacity is determined as follows:

$\phi R_n > R_u$ (AISC 360, B3-1)

$\boldsymbol{\phi R_n / l}$= 6.96 k/in (for 5/16" fillet weld) (AISC 360, Section J2)

$$\boldsymbol{\phi R_n = (6.96)(2.06) = 14.3\ kips > F_{p,fastener} = 5.04\ kips \quad OK}$$

***Component #3 - Embed Plate (Body)***

The embed plate needs to be checked against flexure. The flexural capacity of the embed plate can be calculated using AISC design guidelines for rectangular steel sections in weak axis bending as follows:

$$M_u = \frac{F_p L}{4} = \frac{1.61 \cdot 6''}{4} = 2.41\ kip \cdot inch$$

The capacity of the plate can be found as $\phi M_n$, where $\phi$ is 0.90 and $M_n = M_p = F_y Z$ per AISC 360 (F2-1). It is noted that for rectangular plates, $Z = bt^2/4$. Therefore, in this example b = ($b_{nominal}$ – rod hole) = 8" -1.06" = 6.94".

$$\phi M_n = \phi f_y \frac{bt^2}{4} = 0.9 \cdot 36 \cdot \frac{(6.94) \cdot (0.5)^2}{4} = 14.1\ kip \cdot inch$$

Thus:

$\phi M_n = 14.1\ kips \cdot inch > M_u = 2.41\ kips \cdot inch$ **OK**

***Component #4 - Threaded Rod (Fastener)***

The threaded rod in the connection needs to be checked for both tension and compression. In this case the equations to check the component are found in the AISC code.

*Tension*

The characterization of the tensile strength of threaded parts in pure tension can be found in AISC, Section J3.6. The design tension strength $\phi R_n$ is defined from the nominal tensile stress $F_n$ and the unthreaded area $A_b$. The same section defines $\phi$ as 0.75. The value of $F_n$ is defined as $0.75F_u$ in AISC, Table J3.2 for this type of threaded rod:

$$\phi R_n = \phi \cdot F_n \cdot A_b = \phi \cdot 0.75 \cdot F_u \cdot A_b = 0.75 \cdot 0.75 \cdot 58 \cdot 0.79 = 25.8\ kips$$

(AISC, Equation J3-1)

$$\phi R_n = 25.8\ kips > F_{p,fastener} = 5.04\ kips \quad \textbf{OK}$$

*Compression*

The requirements for design of the threaded rod in compression can be found in AISC, Section E1 – E3. The compression capacity of the rod $P_{nc}$ is found through the critical stress Fcr, which is determined based on the value of the elastic critical buckling stress Fe. The value of Fe is calculated based on the material properties and geometry of the rod, including its length L (29 inch), its radius of gyration r (0.22 inch) and the effective length factor K (1.2, as defined is AISC, Table C-C2.2). It can be found that:

$$\frac{KL}{r} = \frac{1.2 \cdot 29}{0.22} = 158.2 > 4.71\sqrt{\frac{E}{F_y}} = 133.6$$

Thus:

$$F_{cr} = 0.877 \cdot F_e$$ (AISC Equation E3-3)

And:

$$F_e = \frac{\pi^2 E}{\left(\frac{KL}{r}\right)^2} = \frac{\pi^2 \cdot 29000}{(158.2)^2} = 11.44\ ksi$$ (AISC Equation E3-4)

$F_{cr} = (0.877)(11.44\ ksi) = 10.0ksi$

The capacity of the rod in compression can be determined considering a ϕ of 0.9 determined is AISC, Section E1 and assuming the gross area of the member $A_g$ is equal to the threaded area $A_t$ of 0.606 inch$^2$:

$\phi P_{nc} = \phi \cdot F_{cr} \cdot A_g = 0.9 \cdot 10.0 \cdot 0.606 = 5.45\ kips$ (AISC Equation E3-1)

$\phi P_{nc} = 5.45\ kips > F_{p,fastener} = 5.04\ kips$ **OK**

***Component #5 – Plate Washer (Body)***

The plate washer is designed as a simple span beam, which extends over the 3" diameter hole in the supporting plate. Subsequently it is designed similar to the embed plate using AISC design methods for weak axis flexure of rectangular sections.

$M_u = \frac{F_p L}{4} = \frac{1.61 \cdot 3}{4} = 1.21\ kip \cdot inch$

$\phi M_n = \phi f_y \frac{bt^2}{4} = 0.9 \cdot 36 \cdot \frac{(1.94) \cdot (0.375)^2}{4} = 2.21\ kip \cdot inch\ >\ M_u = 1.21\ kip \cdot inch$ **OK**

***Component #6 - Cantilevered Plate (ductile fuse) (Body)***

A drawing of the cantilevered plate, which in the ductile design example serves as the ductile fuse and its applied forces is shown in Figure 3.8. The moment demand $M_u$ on the cantilevered plate can be found as:

$M_u = P_u e = 1.61 \cdot 11.5 = 18.5\ kips \cdot inch$

The capacity of the plate can also be determined using weak axis flexure of rectangular bars as follows:

$\phi M_n = \phi f_y \frac{bt^2}{4} = 0.9 \cdot 36 \cdot \frac{7 \cdot 0.75^2}{4} = 31.9\ kip\ \cdot inch$

Then, it can be verfied that:

$\phi M_n = 31.9\ kip \cdot inch > M_u = 18.5\ kip \cdot inch$ **OK**

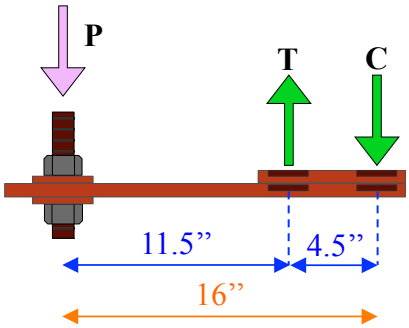


**Figure 3.8. Detail of the connection plate and its applied forces (component 6)**

***Component #7 – Plate Welds (Fastener)***

The tension force T applied to the weld can be found through equilibrium (Figure 3.9).

$T = F_{p,fastener}\frac{16}{4.5} = 5.04 \cdot \frac{16}{4.5} = 17.9\ kips$

The strength of weld metal $R_n$ is defined in AISC, Section J2.4 from the nominal strength of the weld $F_w$ and the weld area $A_w$ as:

$R_n = F_w A_w$ (AISC, Equation J2-3)

AISC Table J2.5 defines that $F_w$ is $0.6F_{EXX}$, where $F_{EXX}$ is the electrode classification number. In addition, the same table defines $\phi$ equal to 0.75. In this case:

$\phi R_n = \phi 0.6 F_{EXX} A_w = 0.75 \cdot 0.6 \cdot 70 \cdot \frac{0.313}{\sqrt{2}} \cdot 4 = 27.8\ kips$

Comparing demand to capacity:

$\phi R_n = 27.8\ kips > T = 17.9\ kips$

It should be noted that the back span welds are conservatively sized to match the cantilever side welds.

***Component #8 – Column Embed Plate in flexure***

The embed plate in the column should be checked in flexure, with load points at the 5/16" fillet welds, and support points at the headed studs. In this example, the studs and welds are nearly concentric, so the bending moment is negligible.

***Component # 9 – Headed Studs in the Column Embed (Fastener)***

The tension force applied to a couple of anchors in tension can be found with equilibrium considerations:

$$T = F_{p,fastener}\frac{16}{6} = 13.4\ kips$$

The same calculation used for the anchors in the panel can be used to check the column embed. The design geometry of this embed are shown in Figure 3.9.

*Concrete Breakout*

The relevant parameters to determine the resistance against concrete breakout are:

- $h_{ef}$ = Plate thickness + stud length – stud head thickness;
    - $h_{ef}$ = 0.75" + 8" – 0.375" = 8.38"
- The modification factors for eccentric load $\Psi_{ec}$, cracking $\Psi_c$ and for post-installed anchors $\Psi_{cp}$ are all equal to 1. Their definition can be found in ACI sections D.5.2.4, D.5.2.6, D.5.2.7.
- Since $c_{a,min} = c_{a1} = 6 < 1.5 \cdot h_{ef} = 12.57$ the modification factor for edge effects can be found as:

$$\Psi_{ed} = 0.7 + 0.3\frac{c_{a,min}}{1.5h_{ef}} = 0.7 + 0.3\frac{6}{12.57} = 0.84 \qquad \text{(ACI equation D-11)}$$

- The anchor is cast-in, thus the parameter $k_c$ is equal to 24; (ACI, Equation D-7)
- The concrete is normal weight, and the corresponding $\ell$ factor is 1.0. (ACI, Section 8.6)

In this case the relevant quantities are:

$$A_{NCO} = 9h_{ef}^2 = 9 \cdot (8.38)^2 = 632\ inch^2 \quad \text{(ACI, Equation D-6)}$$

$$A_{NC} = \left(s_1 + 1.5h_{ef} + 1.5h_{ef}\right) \cdot 18 = 31.2 \cdot 18 = 560\ inch^2$$

$$N_b = k_c \lambda \sqrt{f_c'} h_{ef}^{1.5} = 24\sqrt{5000}\ 8.38^{1.5} = 41.2\ kips \quad \text{(ACI, Equation D-7)}$$

$$N_{cbg} = \frac{A_{Nc}}{A_{Nco}} \Psi_{ec} \Psi_{ed} \Psi_c \Psi_{cp} N_b = \frac{562}{632} \cdot 1 \cdot 0.84 \cdot 1 \cdot 1 \cdot 1 \cdot 41.2 = 30.7\ kips \quad \text{(ACI, Equation D-7)}$$

$$0.75\ \phi N_{cbg} = 0.75 \cdot 0.75 \cdot 30.8 = 17.3\ kips > T = 13.4\ kips \quad \text{(ACI, Equation D-1)}$$

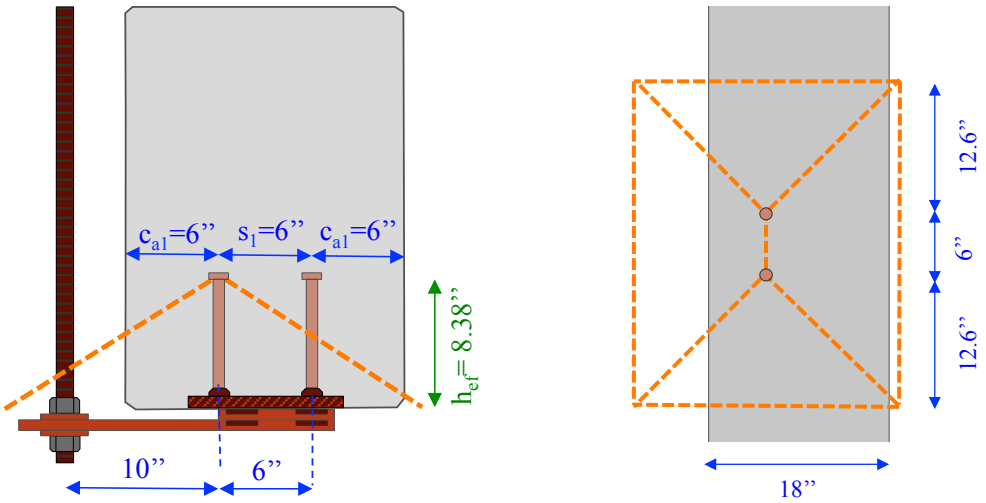


**(a)** **(b)**

**Figure 3.9. Detail of the column embed: (a) plan view and (b) elevation view**

*Steel Anchors*

Two anchors are in tension and their $A_{se,N}$ is 0.44 inch$^2$, thus:

$$N_{sa} = nA_{se,N} f_{uta} = 2 \cdot 0.44 \cdot 65 = 57.2\ ksi \quad \text{(ACI, Equation D-3)}$$

$\phi N_{sa} = 0.75 \cdot 57.2 = 42.9\ kips > T = 13.4\ kips$ (ACI, Equation D-1)

### 3.4.2 Sizing the Corner Joint

***Conventional Design***

In a conventional design, the vertical gap needs to accommodate the allowable story drift $\Delta_a$ as determined from ASCE 7, Table 12-12.1. For a special moment frame 5-story office building (Occupancy Category II):

$\Delta_a = 0.02h$

In the example building, the story height is assumed to be 13', thus:

$\Delta_a = 3.12''$

For a full-story height panel, the tilt of the panel will be equal to the story drift, therefore, to avoid collision, the gap needs to be larger than 3.12''. The vertical gap can be rounded to the nearest quarter of an inch, in other words, the joint width would be defined as 3.25"

***Ductile Design***

If the corner connection is detailed to be ductile, the joint can be allowed to close during inelastic drift. For this case, the joint should be sized for the elastic (reduced) displacements of the structure $D_{p,elastic}$. This can be determined by dividing the allowable story drift $\Delta_a$ by the deflection amplification factor $C_d$, that is equal to 5.5 for special concrete moment frames (ASCE 7 Table 12.2-1):

$$D_{p,elastic} = \frac{\Delta_a}{C_d} = \frac{3.12}{5.5} = 0.56\ inch$$

This $D_{p,elastic}$ is larger than the minimum of 0.5 inch required by ASCE 7, section 13.5.3(a) and would thus govern the size of the joint. However, industry practice is to use ¾" wide joints to accommodate fabrication and erection tolerances. Furthermore, another important consideration is the elastic performance of the sealant used to fill the joint. Many high performance sealants allow a maximum of 50% compression to remain "elastic" or undamaged. This means that in the case under consideration, the sealant width would be 0.56"/0.5 = 1.12" or about 1-1/4" to maintain the sealant warranty.

### 3.4.3 Ductile Fuse Design

For the conventional design case, no additional checks need to be performed, however, in the case of a ductile design there is a final check, namely, the expected forces activating the ductile fuse need to be smaller than the capacities of the other elements in the load path – to ensure the fuse is the element that fails.

The maximum plastic flexural capacity of the cantilevered plate, inluding strain hardening effects and expected material overstrength values can be found in AISC 341 as:

$$M_{p-expected} = 1.1 R_y F_y Z$$

The parameter $R_y$ is the ratio of expected yield stress to the specified yield stress $F_y$ defined by AISC 341, Table A3.1 and is equal to 1.5 for A36 hot-rolled shapes and bars. Thus:

$$M_{p-expected} = 1.1 \cdot 1.5 \cdot 36 \cdot \frac{7 \cdot 0.75^2}{4} = 58.5\ kip \cdot inch$$

$$P_{max} = \frac{M_{p,expected}}{Moment\ arm-min} = \frac{58.5}{10} = 5.85\ kips$$

The parameter $P_{max}$ represents the maximum tension the plate can resist from the rod during the collision event (when the column continues to travel while the panel joint is closed). The moment arm is reduced to the minimum dimension possible (10'' instead of the original 11.5''),

accounting for installation tolerances, so as to create the most conservative force. To verify ductile fuse performance, $P_{max}$ should be less than the capacity of all other elements in the load path, as summarized in Table 3.2.

**Table 3.2. Summary of calculations comparing the demand to capacity of all non-yielding components of the ductile fuse corner connection**

| Component | Failure mode | Demand | Capacity | Check Results |
|---|---|---|---|---|
| Panel embed | Concrete breakout | $P_u=P_{max}$=5.85 kips | $\phi P_n$=16.0 kips | OK |
| | Anchor tension | $P_u=P_{max}$=5.85 kips | $\phi P_n$=39 kips | OK |
| | Headed stud weld fracture | $P_u=P_{max}$=5.85 kips | $\phi P_n$=14.3 kips | OK |
| | Plate flexure | $M_u=P_{max}L/4$=8.78 kip-inch | $\phi M_n$=14.1 kip-inch | OK |
| Rod | Tension | $P_u=P_{max}$=5.85kips | $\phi P_n$=25.8 kips | OK |
| Column Embed | Plate weld fracture | $P_u=P_{max}(16/4.5)$=20.8 kips | $\phi P_n$=27.8 kips | OK |
| | Concrete breakout | $T_u= P_{max}$ (16/6)=15.6 kips | $\phi P_n$=17.3 kips | OK |
| | Anchor tension | $T_u= P_{max}$ (16/6)=15.6 kips | $\phi P_n$=42.9 kips | OK |

It is noted that the rod was checked in tension only because the binding motion occurs only in one direction, when the column pulls the panel with the return leg into the panel around the corner. When the column pushes the panel outward, the joint simply opens and there is no induced force from drift or binding of panels.

# REFERENCES

American Concrete Institute Committee 318, 318-11 (2011). "Building code requirements for structural concrete and commentary", ACI, Farmington Hills, MI.

American Institute of Steel Construction, 341, 341-10 (2010), "Seismic provisions for steel buildings", AISC, Chicago, IL.

American Society of Civil Engineers (2010). "ASCE 7-10 minimum design loads for buildings and other structures", ASCE, Reston, VA.

Arnold, C. (2009). "Seismic safety of the building envelope". Whole building design guide, Accessed at:<http://www.wbdg.org/resources/env_seismicsafety.php>

Baird, A., Palermo, A. and Pampanin, S. (2011). "Façade damage assessment of multi-storey buildings in the 2011 Christchurch earthquake." *Bulletin of the New Zealand Society for Earthquake Engineering*, 44 (4), pp. 368-376.

Bournas, D. A., Negro, P., and Taucer, F. F. (2013). "Performance of industrial buildings during the Emilia earthquakes in Northern Italy and recommendations for their strengthening." *Bulletin of Earthquake Engineering*, June 2013, pp. 1-22.

Chen, M. C., Pantoli, E., Wang, X., Astroza, R., Ebrahimian, H., Hutchinson, T. C., Conte, J. P., Restrepo, J. I., Marin, C., Walsh, K., Bachman, R. E., Hoehler, M. S., Englekirk, R., and Faghihi, M., 2014. "Full-scale structural and nonstructural building system performance during earthquakes: Part I – specimen description, test protocol and structural response." *Earthquake Spectra*.

Chen, M.C., Pantoli, E., Wang, X., Astroza, R., Ebrahimian, H., Mintz, S., Hutchinson, T. C., Conte, J. P., Restrepo, J. I., Meacham, B., Kim, J., and Park, H., 2013a. "BNCS Report #1: Full-scale structural and nonstructural building system performance during earthquakes and post-earthquake fire - specimen design, construction and test protocol." *Structural Systems Research Project Report Series, SSRP 13/9.* University of California San Diego, La Jolla, CA.

Chen, M. C., Pantoli, E., Wang, X., Mintz, S., Hutchinson, T. C., and Restrepo, J. I., 2013b. "BNCS Report #4: Full-scale structural and nonstructural building system performance during earthquakes and post-earthquake fire – construction details and technical

specifications of specific subsystems." *Structural Systems Research Project Report Series, SSRP 13/12*. University of California San Diego, La Jolla, CA

Dao, Nhan Dinh. (2012). Seismic response of a full-scale 5-story steel frame building isolated by triple bearings under 3D excitations. A dissertation submitted in partial bulfillment of the requirements for the degree of Doctor of Philosophy in Civil and Environmental Engineering. University of Nevada at Reno.

Earthquake Engineering Research Institute, EERI (1990). "Loma Prieta earthquake reconnaissance report." *Earthquake Spectra*, Supplement to Vol. 6.

Goodno, B., Craig, J., and Zeevaert-Wolff, A. (1989). "The Mexico earthquake of September 19, 1985-behavior of heavy cladding components." *Earthquake Spectra*, 5(1), pp. 195-222.

Ghosh S.K., and Cleland N.M. (2012) "Performance of precast concrete building structures." *Earthquake Spectra*, 28(S1), pp. S349–S384.

Horii, S., Oka, S., Inukai, M., Kohno, K., Sakamoto, I., Seike, T. (1995). "A report on the damages of precast concrete curtain walls by the 1995 Hyogo-Ken Nanbu earthquake." PCSA, Tokyo, Japan.

Hutchinson T., Restrepo J., Conte J., and Meacham B. (2013). "Overview of the building nonstructural components and systems (BNCS) project." *Proceedings, ASCE Structures Congress*, May 2-4, Pittsburgh, PA, pp. 1485-1498.

International Code Council (2012). "2012 International building code", Country Club Hills: ICC, IL.

Iverson, J.K., and Hawkins, N.M. (1994). "Performance of precast/prestressed concrete building structures during Northridge earthquake." *PCI Journal*, 39(2), pp. 38-55.

McMullin, K. M., Ortiz, M., Patel, L., Yarra, S., Kishimoto, T., Stewart, C., and Steed, B., 2012. "Response of exterior precast concrete cladding panels in NEES-TIPS/NEESGC/E-Defense tests on a full scale 5-story building." *Proceedings, 2012 ASCE Structures Congress*, May 29-31, Chicago, IL, pp. 1069-1079.

McMullin, K. M. (2014). Experimental testing of coil rod under flexural loading for push-pull connections on architectural precast concrete. Report to the Charles Pankow Foundation.

Miyamoto International, (2009). "L'Aquila, Italy, earthquake field investigation report", West Sacramento, CA.

Pantoli, E., Chen, M. C., Wang, X., Astroza, R., Ebrahimian, H., Hutchinson, T. C., Conte, J. P., Restrepo, J. I., Marin, C., Walsh, K., Bachman, R. E., Hoehler, M. S., Englekirk, R., and Faghihi, M., 2014a. "Full-scale structural and nonstructural building system performance during earthquakes: part II – NCS damage states." *Earthquake Spectra* (In review).

Pantoli, E., Hutchinson, T., Underwood, G. A., and Hildebrand M., 2014b. "Seismic behavior of sliding push-pull connections in architectural precast concrete panels." *Proceedings, Façade Tectonics Conference*, January 9-12, Los Angeles, CA.

Pantoli, E., Chen, M., Wang, X., Astroza, R., Mintz, S., Ebrahimian, H., Hutchinson, T., Conte, J. P., Restrepo, J. I., Kim, J., Park, H., and Meacham, 2013a. "BNCS report #2: full-scale structural and nonstructural building system performance during earthquakes and post-earthquake fire – test results." *Structural Systems Research Project Report Series, SSRP 13/10.* University of California San Diego, La Jolla, CA.

Pantoli, E., Chen, M., Hutchinson, T., and Restrepo, J., 2013b. "BNCS Report #3: Full-scale structural and nonstructural building system performance during earthquakes and post-earthquake fire – camera and analog sensor details." *Structural Systems Research Project Report Series, SSRP 13/11*. University of California San Diego, La Jolla, CA.

Pantoli, E., Chen, M., Hutchinson, T., Underwood, G. A., and Hildebrand M., 2013c. "Shake table testing of a full-scale five-story building: seismic performance of precast concrete cladding panels." *Proceedings, Compdyn,* June12–14, Kos Island, Greece.

Pantoli, E., Hutchinson, T., Underwood, G. A., and Hildebrand M., 2013d. "Shake table testing of a full-scale five-story building: seismic performance of precast concrete cladding panels." *Proceedings, PCI convention,* September 21-24, Grapevine, TX.

PCI-Precast/Prestressed Concrete Institute, PCI MNL 120 (2010). "PCI design handbook-precast and prestressed concrete", PCI, 209 W Jackson Boulevard, Suite500, Chicago, IL.

PCI-Precast/Prestressed Concrete Institute PCI MNL 122 (2007). "Architectural precast concrete", PCI, 209 W Jackson Boulevard, Suite500, Chicago, IL.

Ryan, K. L., Mahin, S. A., and Mosqueda, G,. (2008). "Introduction to NEES TIPS: tools for isolation and protective systems. Structures congress." *Proceedings, 18th Analysis and Computation Specialty Conference*, April 24-26, Vancouver, Canada, pp. 1-16.

Sielaff, B. J., Nielsen, R. J., and Schmeckpeper, E. R. (2005). "Evolution of design Code requirements for exterior elements and connections", *Earthquake Spectra*, 21(1), pp. 213-224.

Soroushian, S., Ryan, K. L., Maragakis, M., Sato, E., Sasaki, T., Okazaki, T., Tedesco, L., Zaghi, A.E., Mosqueda, G., and Alvarez, D. (2012). "Seismic response of ceiling/sprinkler piping nonstructural systems in NEES TIPS/NEES nonstructural/NIED collaborative tests on a full scale 5-story building." *Proceedings, 2012 ASCE Structures Congress*, May 29-31, Chicago, IL, pp. 1315-1326.

Taghavi S., and Miranda E. (2003). "Response assessment of nonstructural building elements." *PEER Report 2003/05*, University of California, Berkeley, CA.

Taly, N. (1988). "The Whittier Narrows, California earthquake of october 1, 1987 - performance of building at california state university, Los Angeles." *Earthquake Spectra*, 4(2), pp. 277-317.

Wang, M. L. (1987). "Cladding performance on a full scale test frame", *Earthquake Spectra*, 3(1), pp. 119-173.

# APPENDIX A – MATERIAL PROPERTIES

## A.1 MATERIAL FROM THE BNCS TEST SPECIMEN (SECTION 2.2.1)

Tension tests were performed on two of the batches national coarse threaded rods used for sliding connections in the BCNS project were conducted. The first batch tested consisted of rods initially installed on the building. Herein, these are denoted as the "initial batch". The second batch tested were those rods used to replace all the rods in the in-plane panels following FB3 test. These are referred to as the "final batch". All rods were ¾'' in diameter and the free length of the samples tested was 8''. The tension tests were conducted according to standard ASTM threaded rod tests procedures, with firm grips on either ends and an 110 kip capacity hydraulic load in the MTS 810 material testing system. The exact throat diameters measured for each specimen S1, S2 and S3 for each batch are shown in Table A.1.

**Table A.1. Measured diameters for the specimens tested**

| | **Initial Batch** | | | **Final batch** | | |
|---|---|---|---|---|---|---|
| | S1 | S2 | S3 | S1 | S2 | S3 |
| Measured throat diameter (inch) | 0.646 | 0.645 | 0.647 | 0.640 | 0.640 | 0.640 |

Figure A.1 shows the test apparatus and setup used in the material tests. Output data from the test were the force measured and the corresponding displacement applied by the hydraulic load head and the strain in the central part of the rod as measured by a single extensometer. Because the strain capacity of this sensor was smaller than the strain at bar fracture, this sensor was removed before fracture of the bar. Stress in the bar was calculated from the measured force and the initial diameter of each specimen. The yield stress $f_y$ was found determined using the 0.2% strain offset method. The elongation at fracture of the specimen was determined from the total displacement measured and the initial length of the specimen (8''). Results for the three specimens in terms of $f_y$, $f_u$ and elongation at fracture are shown in Table A.2. As can be seen, results are reasonably consistent for the two batches. The initial batch has an average $f_y$ of 64.6 ksi, while $f_u$ averages 81.6 ksi and the elongation at fracture measured was 13% in all specimens. For the final batch $f_y$ and $f_u$ had an average of 66.3 ksi and 83.6 ksi, respectively and the elongation varied between 14% and 15%. The results in terms of stress-strain and stress-

elongation for the three specimens in the two batches are shown in Figure A.2 and A.3, respectively. It is noted that the small vertical spikes visible in each curve in Figure A.3 were created when the extensimeter was removed.

**Figure A.1. Test apparatus**

**Table A.2. Mechanical properties measured during tension tests**

| | **Initial batch** | | | **Final batch** | | |
|---|---|---|---|---|---|---|
| | S1 | S2 | S3 | S1 | S2 | S3 |
| Yield stress $f_y$ (ksi) | 64.4 | 64.2 | 65.1 | 65.4 | 66.6 | 66.8 |
| Ultimate stress $f_u$ (ksi) | 81.5 | 81.4 | 81.8 | 83.4 | 83.8 | 83.7 |
| Elongation at fracture (%) | 13 | 13 | 13 | 14 | 14 | 15 |

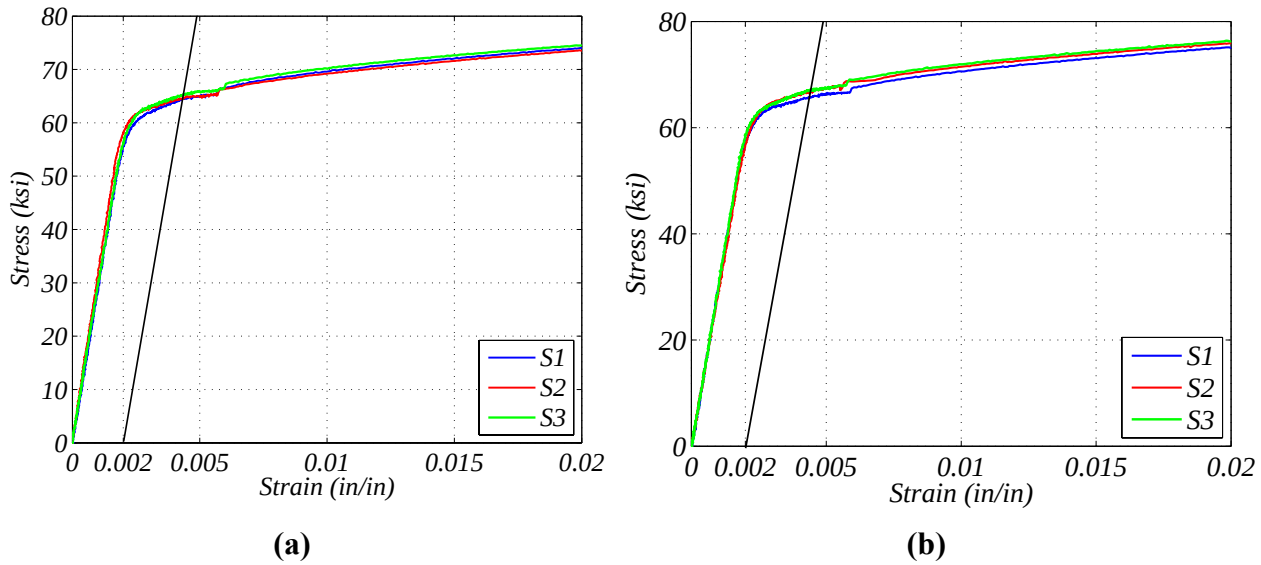


**Figure A.2. Stress-strain curves for strains less than 2% for (a) initial batch and (b) final batch**

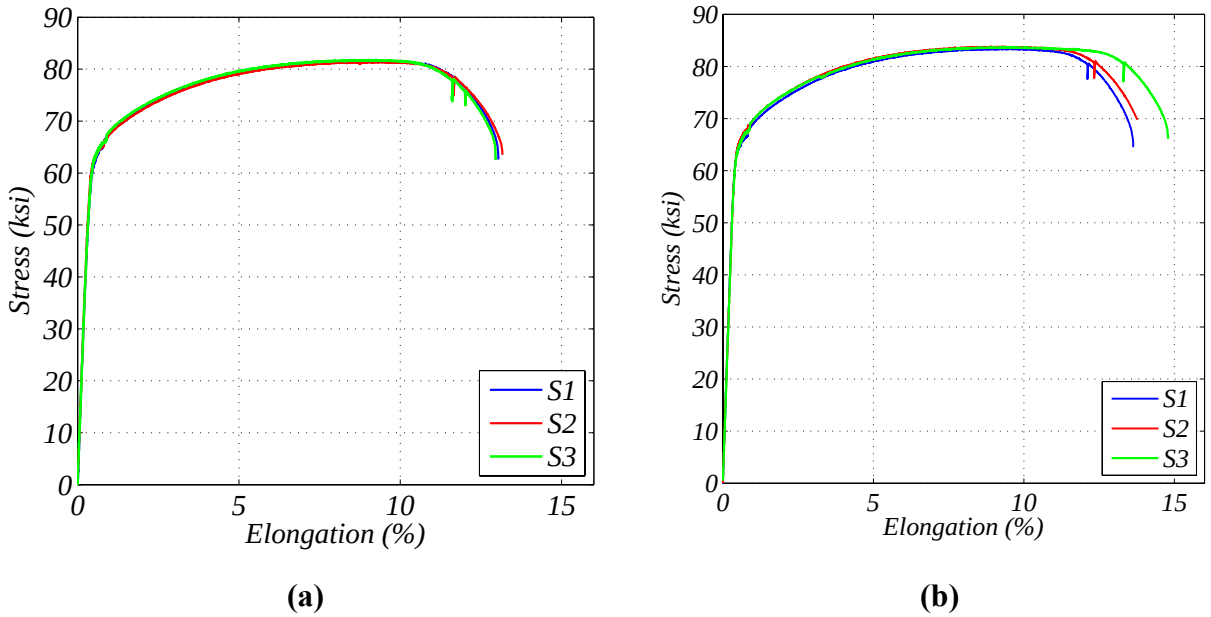


**Figure A.3. Stress-elongation curves for (a) the initial batch and (b) the final batch**

## A.2 COMPONENT TESTS ON FLEXING CONNECTIONS (SECTION 2.2.2)

Mill certificates were provided for the ¾'' diameter coil rod material used in the flexing connection component test. These certificates indicate an average $f_y$ of 48.6 ksi, an average $f_u$ of 71.4ksi and an elongation between 22 and 27%. A summary of the mechanical material

properties reported for the various heat batches is provided in Table A.3. The mill certificate is presented at the end of the chapter.

**Table A.3. Mill certificate results for ¾'' rods used during component test on flexing rod**

| Heat# | $f_y$ (ksi) | $f_u$ (ksi) | Elongation at fracture (%) |
|---|---|---|---|
| 198220 | 49.1 | 71.5 | 22 |
| | 51.5 | 73.0 | 22 |
| 339210 | 47.7 | 70.5 | 27 |
| | 48.0 | 71.5 | 27 |
| 380310 | 48.0 | 71.0 | 27 |
| | 47.5 | 71.0 | 26 |

## A.3 COMPONENT TESTS ON SLIDING CONNECTIONS (SECTION 2.2.3)

Three specimens per rod diameter from material of the same batches of those used in the sliding connection component tests were tested. For each specimen S1, S2 and S3, the initial diameter and free length were measured with a caliper (Table A.4). The test setup and an example of a fractured rod are shown in Figure A.4. The same output data as seen in the tension tests performed on sliding connections for the BNCS test were available in this case. Stress-strain data for the ¾'' diameter rods are shown in Figure A.5a for a strain up to 0.02 (2%). For all specimens $f_y$ as estimated using the 0.2% strain offset method was approximately 60 ksi (exact values are reported in Table A.5). The same results for the three 1'' diameter rod are shown in Figure A.5b. In this case, the yield stress appears slightly lower than 60 ksi. The elongation-stress curves are shown in Figure A.6. The properties of the material calculated with the procedure and data explained above are presented in Table A.5. In summary, for the ¾'' diameter coil rod samples, the average $f_y$ was 59.6 ksi , the average $f_u$ was 72.5 ksi and the elongation at fracture varied from 16 to 19%. For the 1'' diameter rods the average $f_y$ was 58.6 ksi, the average $f_u$ was 79.2 ksi and the elongation at fracture varied form 24 to 26%.

**Table A.4. Measured diameters and free lengths for the six specimens tested**

| | Diameter = 0.75'' | | | Diameter=1'' | | |
|---|---|---|---|---|---|---|
| | S1 | S2 | S3 | S1 | S2 | S3 |
| Measured throat diameter (inch) | 0.64 | 0.64 | 0.65 | 0.87 | 0.86 | 0.86 |
| Measured specimen length (inch) | 5.43 | 5.37 | 5.31 | 5.37 | 5.37 | 5.5 |

**(a)** **(b)**

**Figure A.4. Tension tests on rods used for the component tests on sliding connections: (a) test setup, and (b) example of a fractured rod**

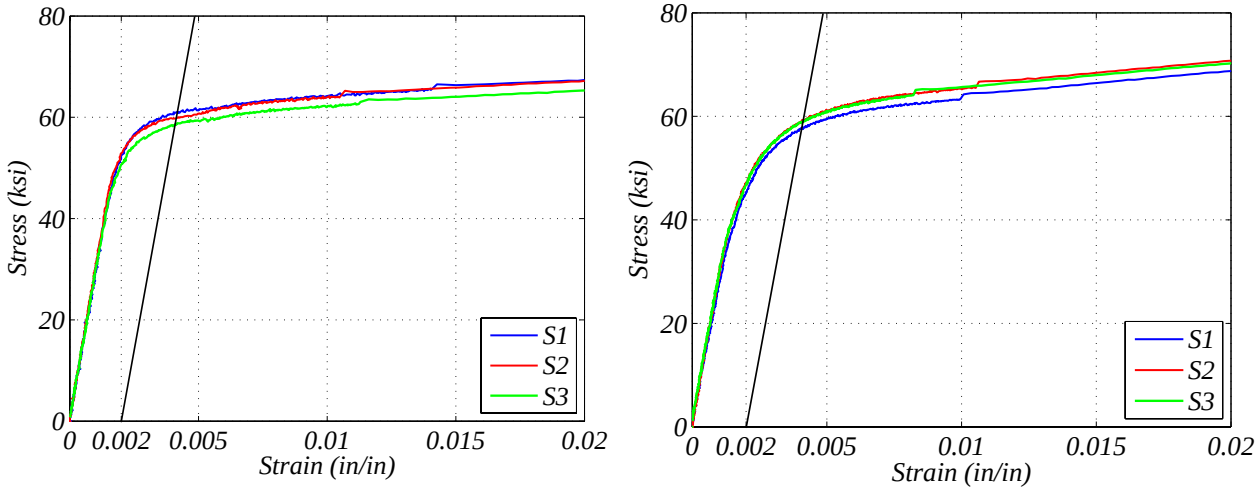


**(a)** **(b)**

**Figure A.5. Stress-strain curves for strains less than 2% for (a) ¾'' diameter rods and (b) 1'' diameter rods**

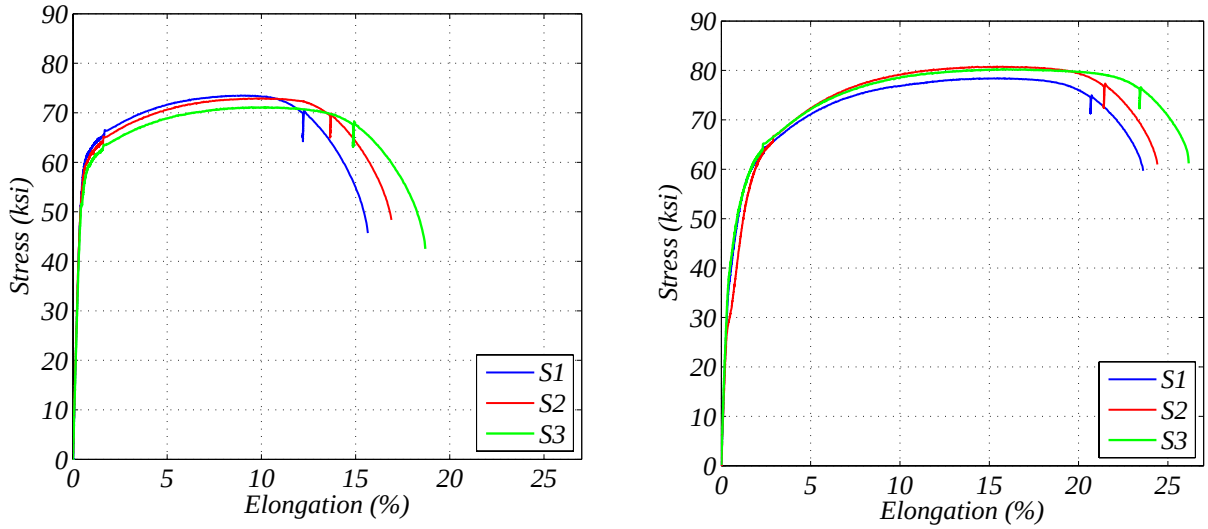


**Figure A.6. Stress-elongation curves for (a) ¾'' diameter rods and (b) 1'' diameter rods**

**Table A.5. Mechanical properties measured during tension tests**

| | **Diameter = 0.75''** | | | **Diameter=1''** | | |
|---|---|---|---|---|---|---|
| | S1 | S2 | S3 | S1 | S2 | S3 |
| Yield stress $f_y$ (ksi) | 61 | 59.7 | 58.3 | 57.6 | 59.2 | 59.1 |
| Ultimate stress $f_u$ (ksi) | 73.5 | 72.9 | 71.1 | 78.4 | 80.8 | 80.2 |
| Elongation at fracture (%) | 16 | 17 | 19 | 24 | 24 | 26 |